UNIVERSITY OF NAIROBI

COLLEGE OF BIOLOGICAL AND PHYSICAL SCIENCE

SCHOOL OF PHYSICAL SCIENCE

CRUSTAL VELOCITY MODEL BENEATH LODWAR STATION, KENYA USING TELESEISMIC P-WAVE RECEIVER FUNCTION

BY

BRUCE KATHURIMA MUTEGI

I56/71712/2011

A DISSERTATION SUBMITTED IN PARTIAL FULFILMENT OF THE REQUIREMENTS FOR THE DEGREE OF MASTER SCIENCE OF GEOLOGY (SEISMOLOGY)

MAY 2014

DECLARATION

This research project is my original work and has not been presented for a degree in any other university.

Signed …… Date……

Bruce Kathurima Mutegi

156/71712/2011

This research project has been submitted for examination with my approval as the university supervisor.

Signed……Date……

Prof Justus Barongo

University of Nairobi

Signed……Date……

Dr Edwin Dindi

University of Nairobi

Signed……Date……

Dr Josphat Mulwa

University of Nairobi

Signed……Date……

Ms Gladys Kianji

University of Nairobi

ABSTRACT

Receiver functions are an important tool to study the structure of the crust and upper mantle including the discontinuities within them. Due to the regional complex geologic history and ongoing tectonism, Turkana area has been a subject of many geophysical studies. These included the KRISP (Kenya Rift International Seismic Project) in the 1980's and 1990's and other studies done by the oil companies. The method used in this research is the receiver function. A receiver function is a seismological technique that exploits the phenomenon of wave conversion. The upcoming P-wave interacts with seismic velocity impedance contrasts below the receiving station to produce polarized P–to- S or P_S converted phases. The time delay between the first arriving P-wave and the P_S converted phase is interpreted to infer the depth of interfaces and the velocity structure directly below the receiver, allowing estimates to be made of the physical properties of the layers. Passive seismic data recorded at the Lodwar seismic station were used in this study. The data were recorded for a period of one year from 1st January, 2012 to 31st December, 2012. A total of 18 teleseismic events were picked for receiver function analysis.

The iterative time domain deconvolution was applied to those teleseismic events. Only the resulting receiver functions with a signal recovery of over 85% were used for subsequent analysis. Reconstructing the local velocity structure by comparing the observed receiver functions with synthetically generated receiver functions is usually regarded as a highly non-linear inverse problem. Forward and inverse methods were used in modeling the receiver functions waveform to obtain the P-wave velocity structure beneath the station. Two major layers were obtained, namely the first layer with a thickness of 10 km and increasing P-wave velocity of 5.75 to 7.25km/s and the second layer with a thickness of 10 km and an increasing P-wave velocity from 6.6 to 8.25km/s whose lower interface coincides with a sharp Moho discontinuity. These results agree quite well with previous geophysical results obtained in the area.

ACKNOWLEDGEMENTS

This study would not have been possible without the support of many people. I would like to express my deepest gratitude to my supervisor, Professor Justus Barongo, who was extremely helpful and offered plentiful assistance and support, and to the other supervisors Dr Edwin Dindi, Dr Josphat Mulwa and Ms Gladys Kianji. Special thanks go to Professor Eric Sandvol of the University of Missouri for his guidance on compilation of receiver function codes. Thanks go to George Githinji for offering his expertise in computer programs installation. I offer my thanks to the all for their continued encouragement and patience throughout this process. I thank the International Science Program, Sweden, through Eastern and southern Africa Seismological Working Group, for offering me a scholarship to undertake these studies. I would further like to acknowledge the rest of the members of Geology Department for their support through this journey.

I would also want to thank IRIS (Incorporated Research Institution for Seismology) for allowing me to download SAC (Seismic Analysis Code) software. Thanks also go to GFZ Potsdam in Germany who helped us set up Lodwar seismic station. The station data have been used to conduct this research. I also thank Comprehensive Test Ban Treaty Organization (CTBTO) for their help in setting up the National Data centre in the Department of Geology, whose facilities were utilized in the completion of this research work

Special thanks go to Ms Cecilia Chiaji, a colleague for taking up my duties at work so that I could comfortably embark on my dissertation and for her help in typesetting this document. Last, but not least, I sincerely thank my family and friends for their support while working on this dissertation and during my education to this point.

TABLE OF CONTENTS

LIST OF FIGURES

LIST OF PLATES

LIST OF TABLE

LIST OF ABBREVIATIONS

IRIS	Incorporated Research Institutions for Seismology
USGS	United States Geological Survey
PRF	P wave Receiver Function
SRF	S wave Receiver Function
PASSCAL	Program for Array Seismic Studies of the Continental Lithosphere
EARS	East African Rift System
KRISPS	Kenya Rift International Seismic Project
CTBTO	Comprehensive Nuclear-Test-Ban Treaty Organization
ORFEUS	Observatories and Research Facilities for European Seismology
GITEW	German-Indonesian Tsunami Early Warning System
GFZ	GeoForschungsZentrum
KBSE	Kenya Broadband Seismic Network
WWSSN	World Wide Standard Seismograph Network
ASCII	American Standard Code for Information Interchange
TCP	Transmission Control Protocol
RMS	Root Mean Square

LIST OF SYMBOLS

P	P wave
S	S-wave
ps	Converted P wave

pmp	P wave reflected at the underside of Moho
Ml,	Local Magnitude
Mb	Body Wave Magnitude
Ms	Surface Wave Magnitude

CHAPTER ONE

1.0 Background of the Study

Geological mapping of the subsurface structures in remote areas is often difficult and very costly. As the depth increases it becomes even more difficult in that the resolution of the data decreases and the cost of the data acquisition generally increase. Many seismic profiling studies aspire to address the structure of the lithosphere, but in fact are primarily studies of crustal structure because of the difficulty and the cost of producing seismic sources which penetrate the mantle. In addition, limits on the number of seismic recording systems available usually force compromises on the resolution if the long-offsets recoding needed for deep penetration are to be obtained (Keller, 1993). The need for other geophysical methods that can probe the upper mantle are sought. One of these methods is the P-wave receiver function analysis, which uses seismic waves generated by a teleseismic earthquake.

The science of Earthquake (Seismology) can be traced back in the mid-1700s with the work of John Michell (Davison, 1978). The use of seismic waves to map the earth structure began in the late 1800 with the advent of seismogram. A seismogram is a record of the time-dependent ground displacement of the earth due to the passage of the seismic waves. It operates on three principles, the source signature, elastic properties of the earth through which the waves are propagating and the detection and recording characteristic of the seismic recorder. When seismic waves are used to map earth structure, a major task is to identify those parts of the seismogram that are due to the elastic response of the earth. It is then possible to use the seismic data to constrain models (mathematical representations) of earth structure.

The natural sources of the seismic waves are the earthquakes on faults at plate boundaries, which radiate compressional (P) waves and shear (S) waves. The particle motion for P waves is in the propagation direction and for S waves the particle motion is perpendicular to the propagation direction. The motion of P and S is described by the wave equation in which scalar and vector potential are used for P and S waves respectively. By Snell's law and the fact that seismic waves velocities generally increase with depth, the paths of body waves bend away from the vertical as they go deeper into the earth; eventually they become horizontal, turn upward and return to

the surface (Stein and Wysession, 2003).The recent availability of 3-component broadband seismic records from Lodwar, Turkana has provided a new opportunity for investigating the structure beneath the area using receiver function analysis.

1.1 Description of the Station Location

The station is located in Turkana County, in the northern Kenya. It borders Uganda to the west, Sudan and Ethiopia to the north, Marsabit and Samburu counties to the east and Baringo and West Pokot counties to the south. The county, whose administrative headquarters is at Lodwar town, is divided into 11 administrative divisions. The actual station location is at longitude 35.3619 °E and latitude 3.4219° N (figure 1.1).

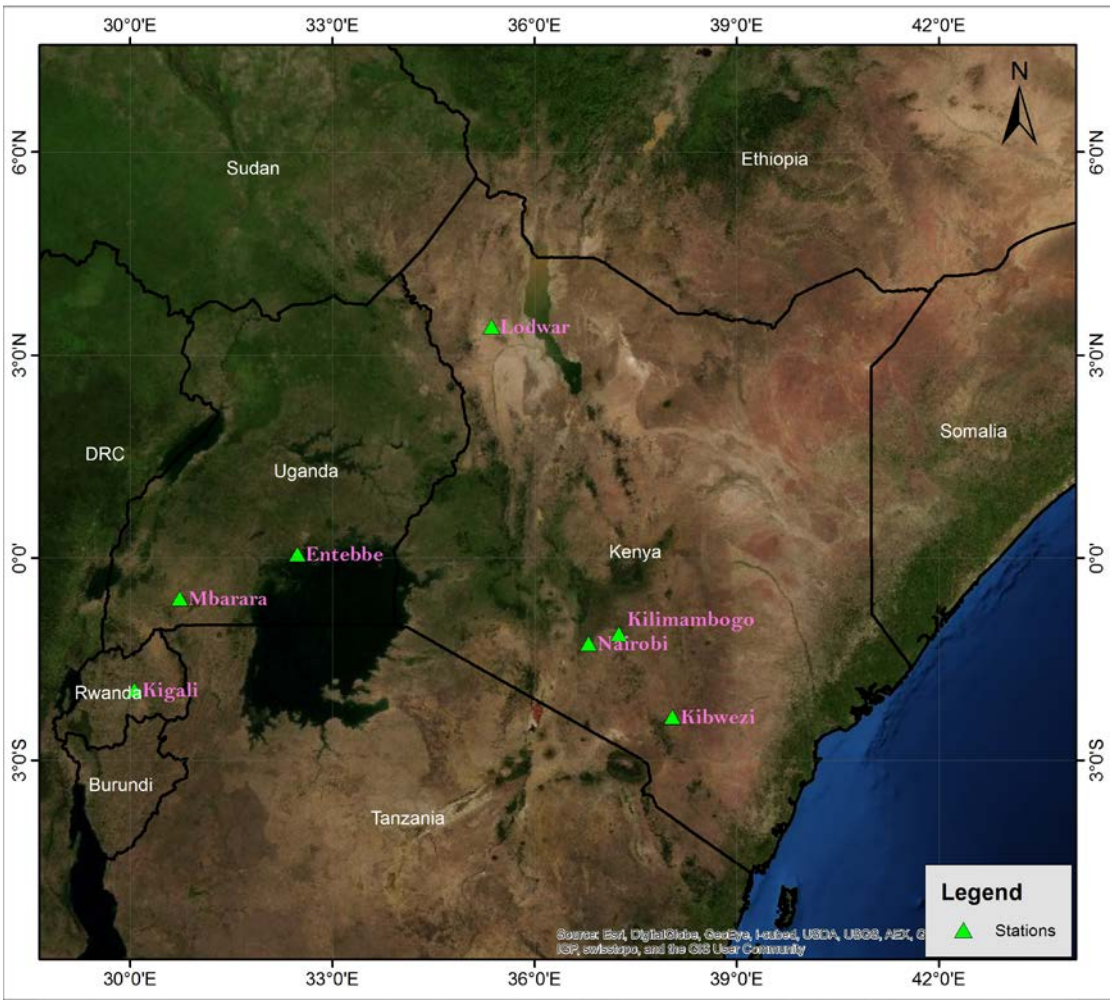

Figure 1-1: Map of seismic stations in Kenya and neighboring countries.

1.2 Topography and Climate

The major topographical features in the county are low-lying plains (plate 1.2 below) interspersed with isolated mountains and hills. Most rivers are seasonal, except Turkwel and Kerio rivers. Volcanic rocks cover about one third of the county. Outcrops from the basement rocks occur in several hills and mountains scattered in the county. The soils are poor and shallow which, combined with low vegetation cover, leads to a rapid run-off after the rains. The altitude ranges from 369 metres at the shores of Lake Turkana to 2067 meters above the sea level at Koilongoi peak. Rainfall amounts range from 120 to 430 mm per annum. The county is classified as arid. The low rainfall is also highly erratic and unreliable. The long rain season occurs between April and August, while the short rains occur in October and November. The district experiences rather high temperatures with a daily average of 24-38°C. The area also experiences strong winds which, together with high temperatures, lead to high evaporation.

Plate 1-1: Dry plain within the Turkana basin close to the Lodwar seismic station location.

1.2.1 Lodwar Station

Lodwar station (plate 1.2) is a GEOFON (Global seismic network of stations) funded by the Germay GFZ project. The station is located within the Turkana basin on

longitude 35.3616°E, latitude 3.4219°N and elevation 665m. The station code name is GE.LODK. The station has the following equipment: Seismometer, Digitizer and VSAT System.

(a)  (b) 

Plate 1-2: (a) Lodwar station entrance and (b) Inside the Lodwar station.

1.2.1.1 Seismometer

The seismometer installed at Lodwar seismic station is a broadband seismometer, which means it is capable of sensing ground motion over a wide frequency band as can be seen in figure 1.2. The sensor is most often used in passive experiments. The flat-to-velocity portion of the bandwidth is generally about 0.01 Hz (100 sec) to 25 Hz.

The measurement is done in a moving reference frame; in other words, the sensor moves with the ground and there is fixed undisturbed reference available. Since the motion of the ground relative to an inertial reference is in most cases much larger than the differential motion within a vault of reasonable dimensions, inertial seismometers are generally more sensitive to earthquakes signals. An inertial seismometer converts ground motion in to an electric signal but its properties cannot be described by a single scale factor, such as output volts per millimeter of ground motion. So displacement cannot be measured directly. According to the inertia principle, we can only observe the motion if it has an acceleration. Seismic wave causes transient motions and this implies that there must be acceleration. Velocity and displacement may be estimated, but inertial seismometers cannot detect any continuous component. Thus seismometer measures the relative motion between the inertial mass and the casing.

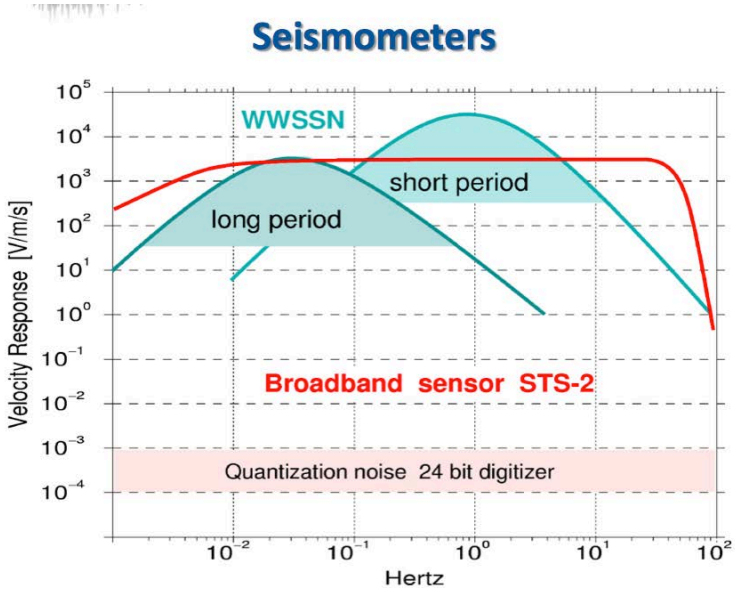

Figure 1-2: Seismometer responses from long period, short period and broadband

1.2.1.2 Digitizer

The type of digitizer at the Lodwar seismic station is **Q330 (**plate 1.3). The **Q330** is a 3 or 6 channel high-resolution datalogger. It is low power and highly configurable for a wide range of applications and sensors. The Q330 is housed in a sealed aluminum enclosure which makes it highly resistant to the environment. Telemetry is a main focus of the Q330, but it also has a robust on-site data storage system which uses external Balers. This makes it easy to swap out the data storage on-site for when servicing doesn't allow an extended visit. The Q330 can write data to four different receiving systems simultaneously. It also has built-in sensor controls, an automatic mass recentering feature, and calibration functions. The Q330 is programmed with a Windows program called Willard; it can also be controlled by a PalmOS program for when working in the field (PASSCAL). Figure 1.3 shows the setup at the station, from the sensor to the digitizer to Vsat. The Vsat is transmits data to receiving satellite.

Plate 1-3: The Q330 digitizer which is used at Lodwar station.

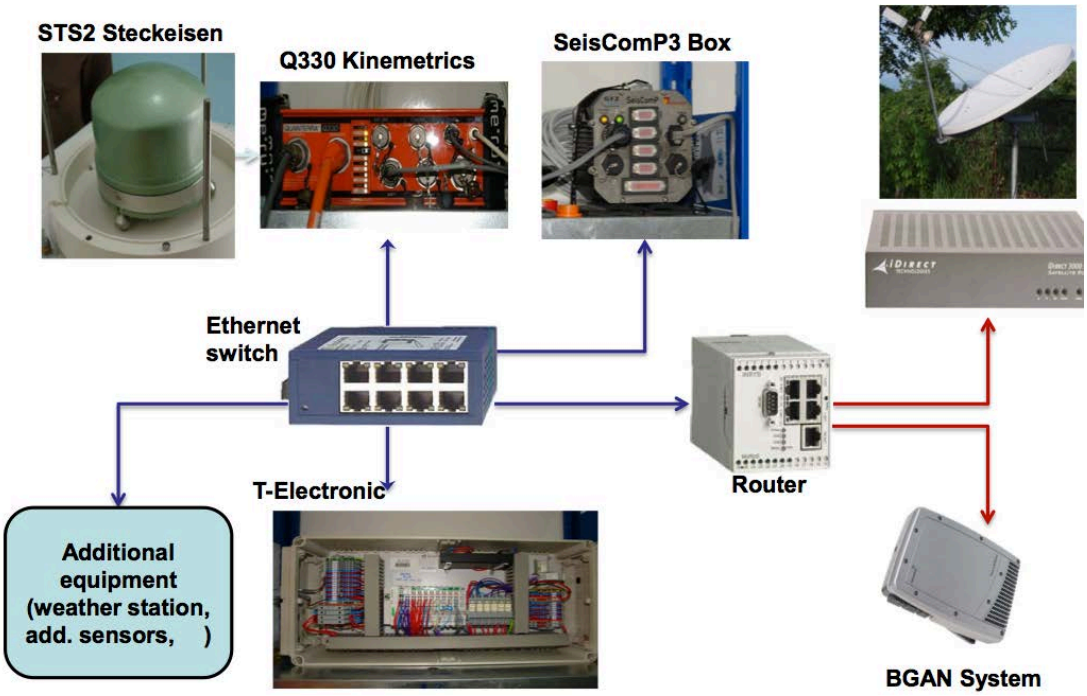

Figure 1-3: Lodwar Seismic station's components modified in

1.3 Problem Statement

Many geophysical methods have been used to study the crust beneath the Turkana basin, they include Reflection, Refraction, Wide-angle and Cross-hole seismic. The cost of these methods is quite high and their spatial coverage is very limited. The techniques named above are used in determining Moho depth from seismic data, the data from these techniques suffers to various degree, the limitation imposed by the

trade-off between the crustal velocity and the thickness. The trade-off can be very severe for those using Moho wide angle reflection and Refraction (PmP and Pn) travel times because these usually travel >100km laterally within the crust. They are much more sensitive to lateral velocity variations than the Moho depth variations (Khu et al 2000). Using the differential travel time between PmP and the first P arrivals can reduce the dependency on the upper crust velocity, but the results are still strongly influenced by lower crustal velocity. In additional picking the secondary PmP is not easy and can sometime be ambiguous. For studies using local earthquakes as energy source, the source location brings in additional uncertainty in the Moho depth estimation. Vertical seismic reflection experiment can reveal fine scale variation of deep crustal structure provided that the energy sources are strong enough to illuminate the Moho. Owing to these challenges an alternative and more effective technique of estimating Moho depth has been developed.

1.4 Aim and Objectives

1.4.1 Aim

The aim of the project is to use seismic data from teleseismic earthquakes recorded on three component broadband station to study the structure beneath the station, by computing series of receiver function.

1.4.2 Specific Objectives

i) To investigate the seismic velocity structure of the crust and upper mantle beneath seismic station.

ii) To produce a crustal model based on the receiver function method and compare with those results obtained during the previous studies.

1.5 Literature Review

The Cenozoic East African Rift System (EARS) has developed primarily within the mobile belts and forms two branches (eastern and western). In Kenya, the Eastern Branch is locally referred to as the Kenya or Gregory Rift, and the uplifted and volcano-capped regions away from the Kenya Rift are referred to as the Kenya Highlands. The Eastern Branch of the EARS formed within the Mozambique Belt,

which runs from south from Ethiopia through Kenya, Tanzania and Mozambique, and is often considered as a Himalayan- type continental collision zone (Burke and Sengor, 1986; Shackleton, 1986). Much of the early work focused on Kenya because the Cenozoic rift structures are well developed there, and field studies were easier to conduct than in other parts of East Africa. For instance, the crustal and upper mantle structure was investigated by the Kenya Rift International Seismic Project (KRISP) between 1985 and 1990 (Fuchs et al., 1997; Prodehl et al., 1994).

More recently, a number of seismic investigations of crustal and upper mantle structure in Tanzania and Ethiopia have yielded important new information, helping to fill in gaps in our knowledge of both lithospheric and sub-lithospheric structure beneath the plateaus (e.g., Last et al., 1997; Nyblade et al., 2000; Owens et al., 2000; Nyblade, 2002; Dugda et al., 2005; Benoit et al., 2006; Yirgu et al., 2006. One approach that has been used successfully to image crustal and upper mantle structure in Tanzania and Ethiopia employs a joint inversion of P wave receiver functions and Rayleigh wave phase and group velocities (Julià et al., 2005; Dugda et al., 2007). From the 1-D S-wave velocity models obtained, estimates have been made of crustal thickness and lithospheric thermal structure. The lithospheric mantle across the centre of the East African Plateau is characterized by Vs values of 4.6 to 4.7 km/s extending to depths of 100 to 150 km or deeper, suggesting that there has been limited, if any, thermal modification of the lithosphere (Julià et al., 2005).

The lithospheric structure of the geologic terrains outlined above has been investigated using a variety of techniques, including body and surface wave tomography (James et al., 2001; Fouch et al., 2004; Priestley et al., 2006; 2008; Li and Burke, 2006; Pasyanos and Nyblade, 2007), inversion of surface wave phase velocities (Freybourger et al., 2001; Weeraratne et al., 2003; Larson et al., 2006), regional waveform modeling (Priestley and McKenzie, 2002; Wang et al., 2008), joint inversion of P-wave receiver functions (PRFs) with surface wave dispersion (Julià et al., 2005; Dugda et al., 2007.

The earliest volcanism in Kenya started in the Turkana region of northern Kenya ca. 35–40 Ma (Furman et al., 2006; MacDonald et al., 2001). Magmatic activity in other parts of northern Kenya began ca. 30 Ma (Morley et al., 1992; Ritter and Kaspar, 1997), while volcanism started ca. 15 Ma in the central portion of the Kenya rift, at

ca. 12 Ma in southern Kenya (Morley et al., 1992; Hendrie et al., 1994; Mechie et al., 1997), and at ca. 8 Ma in northern Tanzania (Dawson, 1992; Foster et al., 1997). Data used for the seismic analyses came primarily from three temporary deployments of broadband seismic stations in eastern Africa. In the year 1994–1995 Tanzania broadband seismic experiment consisted of 20 stations deployed in two more or less linear arrays spanning Tanzania (Nyblade et al., 1996). The 2000–2002 Kenya broadband seismic experiment consisted of 10 stations deployed across central and southern Kenya, and the Ethiopia broadband seismic experiment consisted of 27 stations deployed across central and northern Ethiopia (Nyblade and Langston, 2002).

The method developed by Julià et al. (2003) for the joint inversion was applied to the seismic data from Tanzania (Julià et al., 2005), Kenya (Dugda et al., 2009), and Ethiopia (Dugda et al., 2007). Rayleigh wave group velocities between periods of 10 and 45 s from Pasyanos (2005), and Rayleigh wave phase velocities between periods of 50 and 140 s from Weeraratne et al. (2003), were used in the joint inversion for the data from Tanzania and Kenya (Dugda et al., 2009; Julià et al., 2005). The P wave velocity structure of the crust and upper mantle beneath Kenya has been studied extensively (e.g., Prodehl et al., 1994; Fuchs et al., 1997; Green et al., 1991; Achauer et al., 1994; Slack et al., 1994; Achauer and Masson, 2002; Davis and Slack, 2002; Park and Nyblade, 2006). Six of the seven seismic stations were located either on the eastern or western side of the Kenya Rift and one station was situated within the Kenya Rift. Data from another five stations of the KBSE were not of sufficient quality to be modeled using the joint inversion method. Nyblade and Langston (2002) provide details on the station configuration and recording parameters used in the KBSE.

In joint inversion scheme, P wave receiver functions and fundamental mode Rayleigh wave phase and group velocities are used. The two kinds of data provide complementary information on the earth structure. Receiver functions are time series obtained by deconvolving the vertical component of the teleseismic P-wave coda from the corresponding radial component and can be used to resolve velocity contrasts and relative travel times in the neighborhood of a seismic station (Langston, 1979; Ammon et al, 1990; Julià et al., 2000). Rayleigh wave phase and group velocities, on the other hand, can be used to constrain the average shear wave velocity with depth (Julià et al., 2000; Takeuchi and Saito, 1972).

CHAPTER TWO

2.0 GEOLOGY, TECTONIC SETTING AND SEISMICITY

2.0.1 Geological Setting

The geology of the study area is mainly composed of the basement rock system, (figure 2-1) metamorphic rocks, volcanic and the sedimentary rocks. The basement system rocks of the area consist mainly of semi granitized psammitic sediments, but in the Labur hills semi–pellitic gneisses and crystalline limestones are well developed, with abundant amphibolites and lesser pegmatites. Turkana Grits, which unconformably overlie the basement system rocks, are a succession of sediments which locally exceed 153 meters in thickness. The series is made up of conglomerates, quarzites, sandstones (plate2.2) and minor shales, which thin out northwards and westwards from the lake region to where younger lavas directly overlie the basement system.

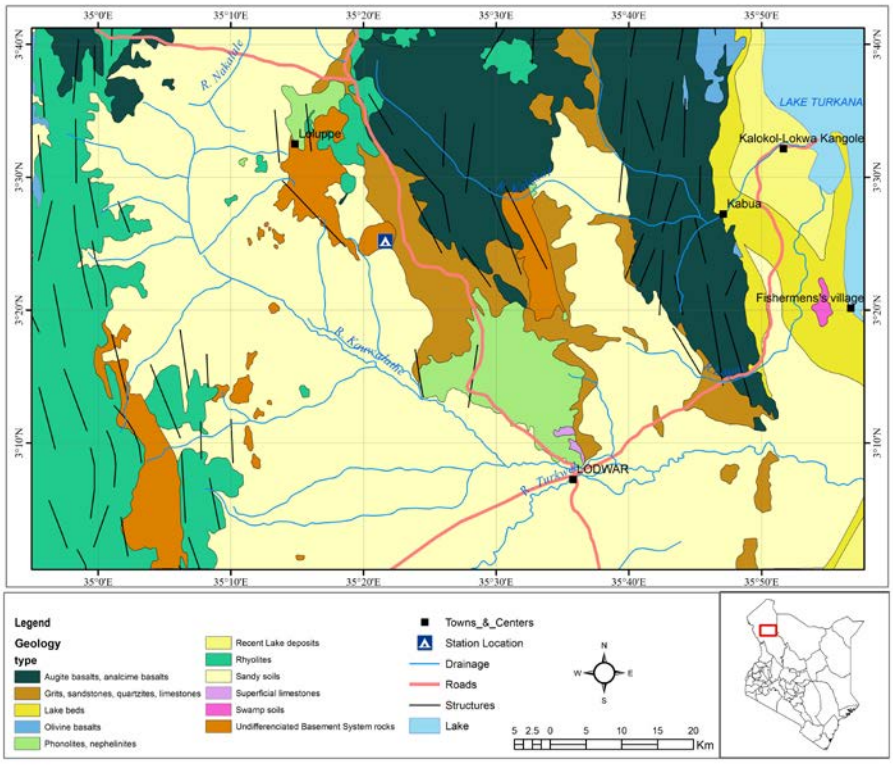

Figure 2-1: Geological map of study area (modified from Dodson Geology of the area south of Lodwar).

2.0.2 Basement system

The oldest rock deposits of the area are metamorphosed, mainly sediments of the basement system, considered to be Precambrian in age. They outcrop in the west of the area along most of the length of the Uganda escarpment, in the north-east along the eastern part of the Labur Hills, and scattered outcrops in the south-centre of the area.

The fault cutting granitoid gneisses at the eastern foot of Muruasigar, has a down throw of nearly 914 meters, it is surprisingly free of brecciation and mylonization. Faulted inlier of basement system rocks occur north of Lodwar and consist mainly of leucocratic granitoid and semi-granitiod rocks mainly of biotitic varieties but toward the east of the outcrop coarse flaggy quartzo-felspathic gneisses with garnet become a dominant rock type.

2.0.3 Metarmorphic rocks

The metamorphic rocks of Turkana are fairly high grade and appear to have been formed from sediments and igneous rocks. Evidence of this is not only in the quartzo-biotite-hornblend schist exposed at the range of the Labor range but more especially in Kaputir and Lokwamur regions. The quartzo-biotite schist in Lapur area strongly contorted, they dip about 45º to the east. Large fragments of gneisses and schicts have been caught up and included in the later-formed rock which exhibits a strong flow structure around these inclusions. The single augens are as much as 0.9M in diameter and the original banding in certain fragments of hornblende gneiss is still preserved. In Kaputir specimen collected vary from massive hornblende schist to hornblende garnet schist. Other rocks found in Kaputir include the marble, garnitiferous schists containing much staurolite.

2.0.4 Turkana Grits

The Turkana Grits were deposited on an eroded locally faulted basement system of rocks. They were deposited in a lacustrine basin as shown by such features as current bedding, layers of well-rounded pebbles and the presence of calcareous mudstones, grits and shales found in the present area. South of Muruangapoi hills and underlying the lava hill on which the town of Lodwar is built, Turkana Grits again outcrop, and

can be traced southwards in the banks of the Turkwel river. North –east of Lodwar on the east flank of the Muruangapoi Hills exposures are generally poor, consisting of pale grey-brown sandy clay capped by pebbly grit.

Plate 2.2. Sandstone rock found within the study area.

The Turkana grits preceded the earliest Tertiary volcanic activity; this is proved by the absence of any volcanic material in the series.

2.0.5 Volcanic Rocks

Most of the mountain ranges and groups of hills are composed of a series of lavas and intercalated pyroclatics erupted during a prolonged phase of volcanicity which followed the early Miocene sedimentation Walsh (1969). The contact between the Turkana grits and the lower basalt is usually disconformable with a small degree of dissection of grits before the lava was emplaced.

The rock overlying the Turkana grits are the volcanic, Arambourg (1935) has made out the following succession for the eruptive rocks in Turkana.

I. Nepheline-syenite
II. Basalts, with interbedded tuffs
III. Phonolites
IV. Rhyolites

On the west of the Lake Turkana the basalts lie directly on the Turkana Grits but include a series of tuffs and ashes which were evidently laid down in rather shallow water under arid conditions. Rhyolites which overlie the more basic volcanic series

are very distinctive in the area; they are localized on the west and north-west of the lake. The Gregory dating placed them in the upper Miocene. This is supported by the local evidence supplied by the tree trucks and wood found in the rhyolitic tuffs.

2.0.6 Tectonic Setting

This site is tectonically unusual within this region in that it has had a prolonged rifting history. Earliest documented rifting began to the east of the modern rift axis when the Anza graben developed during the Cretaceous. Reactivation of existing Anza faults and formation of new grabens have both occurred in Neogene time. Miocene–Recent fault systems initiated in the Lotikipi basin around 25Ma have generally propagated south- eastward through time to the Kinu Sogo fracture zone, the southern terminus of the main Ethiopian Rift. Seismic surveys carried out by Project PROBE, however, found a significant rift structure underlying Lake Turkana (Dunkleman et al., 1988) that suggests the area is a northern continuation of the Kenya Rift (Morley et al., 1992; Hendrie et al., 1994).

This modern rift is characterized by a series of half-grabens that alternate polarity along the length of Lake Turkana. Individual rift basins are approximately 20km long and 10km wide, and Quaternary volcanism occurs at basin midpoints, forming discrete volcanic centers that are axially aligned with a spacing of 51±6km (Dunkleman et al., 1988). The modern Turkana rift is about 150km wide. The superposition of three distinct rifting episodes in North Kenya (Late Jurassic–Cretaceous, Paleogene and Miocene–Recent) has produced cumulative stretching factors approaching two (Ebinger & Ibrahim, 1994). Maximum stretching factors calculated for episodic extension in Turkana increase from ~1.25 for the Paleogene to ~1.4 at the end of the Miocene, and reach a maximum value of ~1.6 for the late Pliocene (Hendrieet al., 1994). The cumulative stretching factor approaches the theoretical limit for decompression melting during adiabatic upwelling of asthenosphere of ‘normal’ potential temperature (1280° C; McKenzie & Bickle, 1988), but the episodic values are substantially lower. These observations suggest that a region of elevated mantle temperatures has been needed to generate basalt lavas throughout the history of Turkana magmatism (Tanya et al., 2004).

2.0.6.1 Structure of the Turkana basin.

The rocks in Turkana basin generally strike North-South with both easterly and westerly dips and lineation's showing marked plunges both north and south. The faults of the area appear to be normal faults with the possible exception of that along the eastern margin of the labor Hills. Few of the faults cutting lava show pronounced brecciation. The well exposed faults from the eastern part of the 200-km-wide Turkana rift basin, comprises a series of horsts and grabens within an arcuate 40-km-wide zone that dissects Miocene–Pliocene lavas overlying an earlier asymmetric fault block. The fault belt is ∼150 km long and is bounded to the north and south by transverse (N50°E and N140°E) fault zones (Morley et al., 2005). An unusual feature of the fault system is that it accommodates very low strains (<1%) and since it is no older than 3 Ma, it could be characterised by extension rates and strain rates that are as low as ∼0.1 mm/yr and 10^{-16} s^{-1}, respectively (Morley et al., 2005).

Despite its immaturity, the fault system comprises segmented fault arrays with lengths of up to 40 km, with individual fault segments ranging up to ∼9 km in length. Fault length distributions subscribe to a negative exponential scaling law, as opposed to the power law scaling typical of other fault systems. The relatively long faults and segments are, however, characterised by maximum throws of no more than 100 m, providing displacement/length ratios that are significantly below those of other fault systems. The under-displaced nature of the fault system is attributed to early stage rapid fault propagation possibly arising from reactivation of earlier underlying basement fabrics/faults or magmatic-related fractures. Combined with the structural control exercised by pre-existing transverse structures, this demonstrates the strong influence of older structures on rift fault system growth and the relatively rapid development of under-displaced fault geometries at low strains.

2.0.7 Seismicity

2.0.7.1 Instrumentally Recorded Seismicity

Instrumental monitoring of the earthquakes in Kenya started in 1963 with the installation of the WWSSN- Station (world Wide Standard Seismograph Network) at Chiromo Campus University of Nairobi, by the United State Geological Survey (USGS) This single station was not enough to monitor the seismicity within the

country. In order to monitor local seismicity, it became necessary to install other earthquake station in various part of the country. The University of Nairobi and the University of Karlsruhe (Germany) entered in a working agreement in the year 1989 whose objective was to strengthen the earthquake monitoring capability in the country and encourage more research in the area of earthquake hazards. Five stations were installed in the following areas: Langata, Magadi, Meru, Kibwezi and olkaria.

The sensors type that was installed in these stations was the mars 88 sensor. In the year 1995 the Nairobi station was moved to Kilimambogo National Park. The station is a part IRIS network. The Kilimambogo seismic station is equipped with broadband seismometer and Episensor for strong ground motion monitoring. The data is continuous recorded at the station and transmitted through the satellite to United State of America and to Department of Geology University of Nairobi. In the recent years the preparatory commission for the Comprehensive Nuclear-Test –Ban Treaty Organization set up a seismic monitoring station in Kenya. The station was set up in Kilimambogo the same site with the IRIS station. The station is equipped with an STS-2 sensor which is a broadband sensor and the data is sent to Vienna in Austria and the Department of Geology via satellite.

In the year 2010 the GFZ Potsdam in German in collaboration with University of Nairobi and Kenya Meteorological Department agreed to set up two stations in Kenya for Tsunami early warning system. These two stations were Kibwezi and Lodwar station. Kibwezi had been initially set up but it was vandalized. The sensors installed in these stations were broadband STS 2 seismometers and the data is transmitted via a satellite to Potsdam in German and to the Department of Geology. The data from Lodwar station has been used in this study. The seismicity of the country is as shown in the figure 2-2. From this figure most of the seismic activity is concentrated on the southern part of Kenya and also in central rift valley.

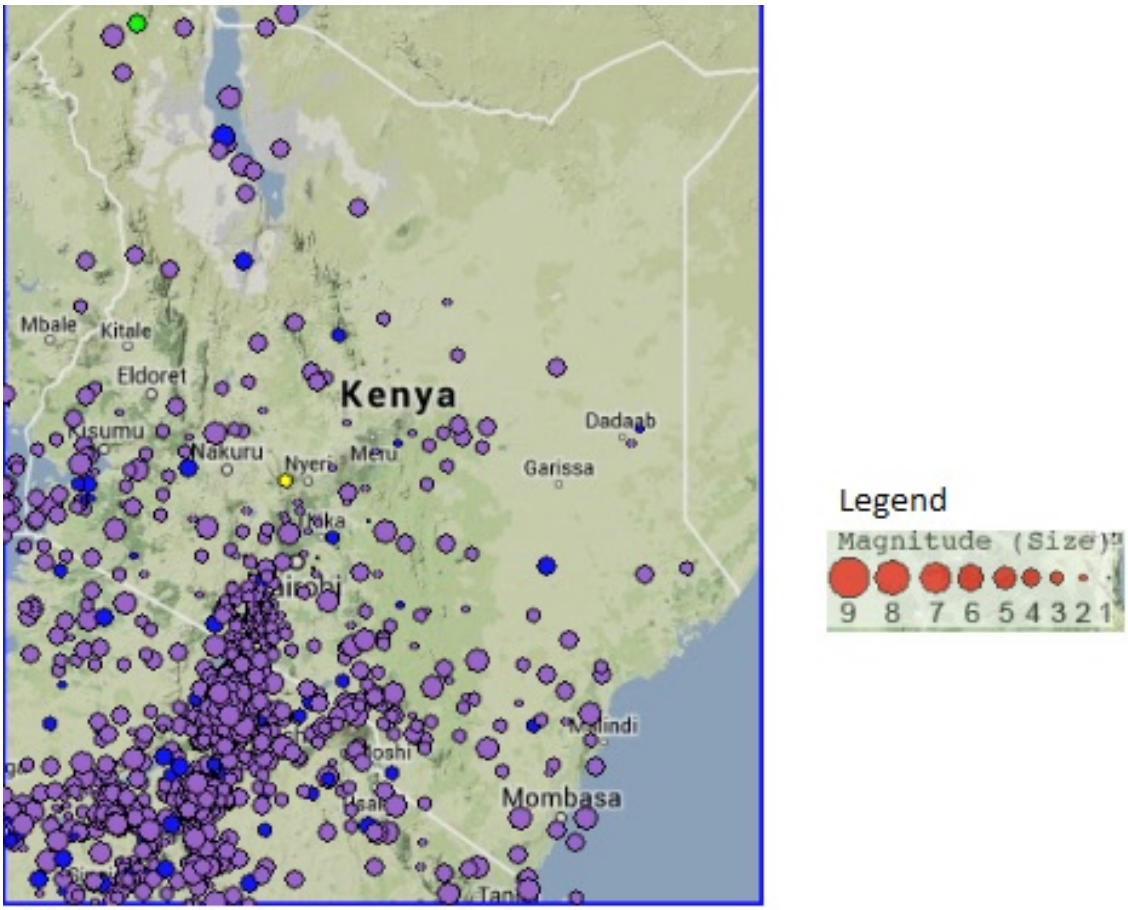

Figure 2-2: Seismicity of Kenya and part of its Neighbors (modified from IRIS)

CHAPTER THREE

3.0 RECEIVER FUNCTION PRINCIPLES

Receiver function analysis is a well -established technique to determine crustal and upper mantle structures using the data of three-component broadband seismograms, and several methods are available for estimating RFs from seismic data.

Probably the most important seismic phase for the receiver function method is a Ps converted wave near a seismometer, or "receiver", to estimate crustal structure (Vinnik, 1977; Langston, 1979). Such P-to-S phase conversion typically occurs at the Moho discontinuity. A P wave with non-perpendicular incidence at a near-horizontal Moho interface generates a transmitted P-wave and a converted Ps phase. The arrival time difference between the P and Ps waves at the surface is proportional to their travel distance or Moho depth. A necessary part of the analysis is to distinguish between the initial P wave and the following P_S converted phase (figure 3-1).

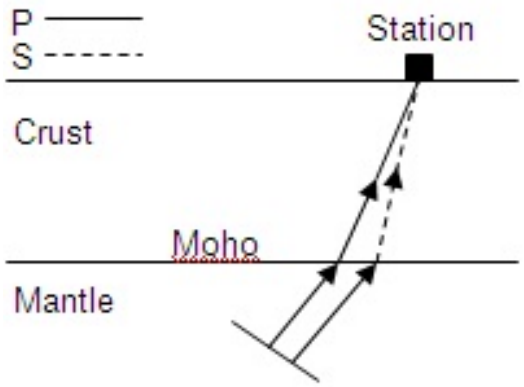

Figure 3-1: Illustration of incident and transmitted waves. When an incident P wave arrives at the Moho from below, some P wave energy will be converted to Ps (P-to-S) wave energy. The arrival time difference between the P and converted Ps waves is proportional to the travel distance between the Moho and the station.

Earthquake ground motion records usually consist of three components: one vertical and two horizontals. Identifying the P wave from the seismic records is relatively easy as the first-arriving wave and usually associated with the largest amplitude on the three components. In addition, the vertical component for an incidence angle less than 45° is usually dominated by the incident P wave. Finding the Ps phase is more difficult since it is often submerged in the coda (including noise or reverberations of complex lithospheric structures) or overlaps with the P wave. The Ps phases are

usually most clearly recorded on the horizontal components, often presented as perpendicular (tangential or SH) and parallel (radial or SV) to a line between the seismometer or seismic station and the epicenter, and conventionally rotated into the great-circle distance using their back azimuth (figure 3-2). The Ps arrival can be enhanced through the construction of the Receiver Function, by deconvolution of the vertical component from the horizontal components which essentially minimize the contributions from the source and enhance the contributions from the crustal structure. In this study we will focus on the radial-component Receiver Function. Using the arrival time difference between the P and Ps waves from the Receiver Function, it is possible to estimate the Moho depth below the station Langston (1979).

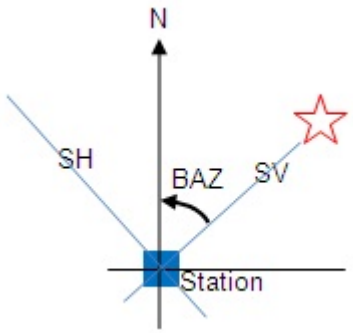

Figure 3-2: Illustration of two horizontal components, perpendicular (tangential or SH) and parallel (radial or SV) to the line from a station to an epicenter (at the star). These two components are rotated into the great-circle distance using their back azimuth angle (BAZ) before deconvolution.

Langston's 3-D raytracing method (Langston 1979) is implemented in both approaches, where structure beneath the receiver is parameterized with a stack of planar, homogenous layers of finite thickness and arbitrary strike and dip (horizontal layers are used for this study). The objective is to reach an estimate of the shear velocity distribution beneath the seismic station by attaining a best fit waveform match between the observed and synthetic waveforms, the latter being the result of raytracing through the parameterized earth model. The final earth model yields the best waveform match, and is a modified version of a starting model into which all available a priori information has been incorporated.

The direct teleseismic P-wave interacts with velocity interfaces and gradients beneath the seismograph to produce a seismogram consisting of the direct P-wave plus P-wave reverberations, and P-to-S converted phases plus their reverberations. An effective procedure to isolate these local Earth structure effects, the source

equalization procedure, has been proposed and discussed by Langston (1979). In this procedure, the three components of the seismic response at any one receiving station caused by the incidence of a plane P-wave, *D(t),* can be theoretically represented in the time domain by

$$D_V(t) = I(t)*S(t)*EV(t)$$
$$D_R(t)=I(t)*S(t)*ER(t) \text{ ……..1}$$
$$D_T(t) = I(t)*S(t)*ET(t)$$

where subscripts *V*, *R* and *T* represent vertical, radial and tangential components respectively; *I(t)* is the impulse response of the recording instrument; *S(t)* is the seismic source function; *E(t)* is the impulse response of the local Earth structure; asterisks represent the convolution operator. *S(t)* may be complicated since it is related to dislocation time history and source area reverberations. Given that the Earth structure beneath a station will produce phase conversions of the P-to-S type, the horizontal components of ground motion will, in general, be quite different from the vertical component (Xuelin et al 2002).

3.1 Receiver Functions Methodology

3.1.1 The Earth structure

The structure of the earth (Figure 3.3) has been studied for over 200 years, and the overall structure is known from analyzing the seismic waves. The interior of the earth is stratified as seen in table 3.1. The earth is said to have a radius of 6371 km. The interior of Earth is divided into five important layers. These are crust, upper mantle, lower mantle, outer core, and inner core. The geologic component of layers and there depths below the surface are as follows:

Table 3-1: Depth of the earth kilometers from the surface to the interior of the inner core (from Anderson, Don L., Theory of the Earth: Boston, Blackwell Publications, 1989).

Kilometers	**Layer**
0–60	Lithosphere (locally varies between 5 and 200 km)
0–35	Crust (locally varies between 5 and 70 km)
35–60	Uppermost part of mantle
35–2,890	Mantle
100–200	Asthenosphere
35–660	Upper mesosphere (upper mantle)
660–2,890	Lower mesosphere (lower mantle)
2,890–5,150	Outer core
5,150–6,360	Inner core

This dissertation focuses on the boundary between the crust and the mantle. A Croatian seismologist named Adrija Mohorovičić discovered this boundary in the year 1909. This is when he observed that seismograms from shallow-focus earthquakes had two sets of *P*-waves and *S*-waves, one that followed a direct path near the earth's surface and the other refracted by a high velocity medium. The Moho mostly lies entirely within the lithosphere; only beneath mid-ocean ridges does it define the lithosphere – asthenosphere boundary. The Moho is typically found in depths around 30-60 km beneath the continents and 5-9km beneath the oceans.

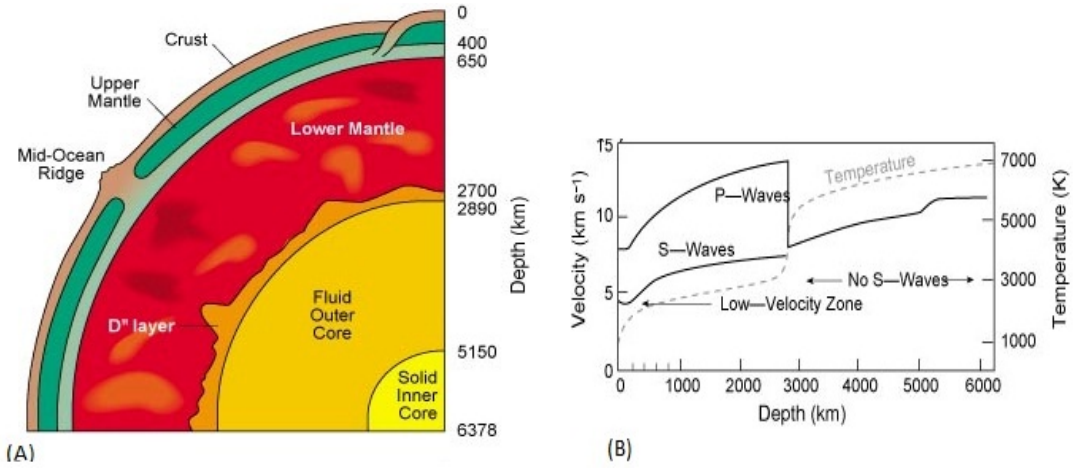

Figure 3-3: (A) The composition of the earth interior and the depth to various layers and (B) the P and S wave velocity model versus the depth(image courtesy Univ. of Hawaii).

When an earthquake occurs, the ground is suddenly shifted inside the earth. The coordinate of the point-like earthquakes is called a hypocenter and the projection on the surface is called an epicenter. When an earthquake occurs, a movement at the hypocenter creates waves in the ground. Two types of waves namely P-waves and S-waves are generated. The P-waves or primary waves are compressional pressure waves with volumetric disturbances much like sound waves as in (Figure 3-4a). The P-waves are the fastest wave type and hence the first to arrive at the seismic station.

The S-waves also known as shear waves are waves that contain only shearing deformation without change in volume. The particle motion in an S-wave is perpendicular to the direction of the propagation of the wave and S-waves cannot exist in fluids. Furthermore S-waves are the second fastest wave type and for the same reason they are called secondary waves (Figure 3-4b). Seismic waves are recorded as time series of the movement of the earth, and such a time series is called a seismogram. The movement is usually recorded in three directions, vertical, East-West and North-South.

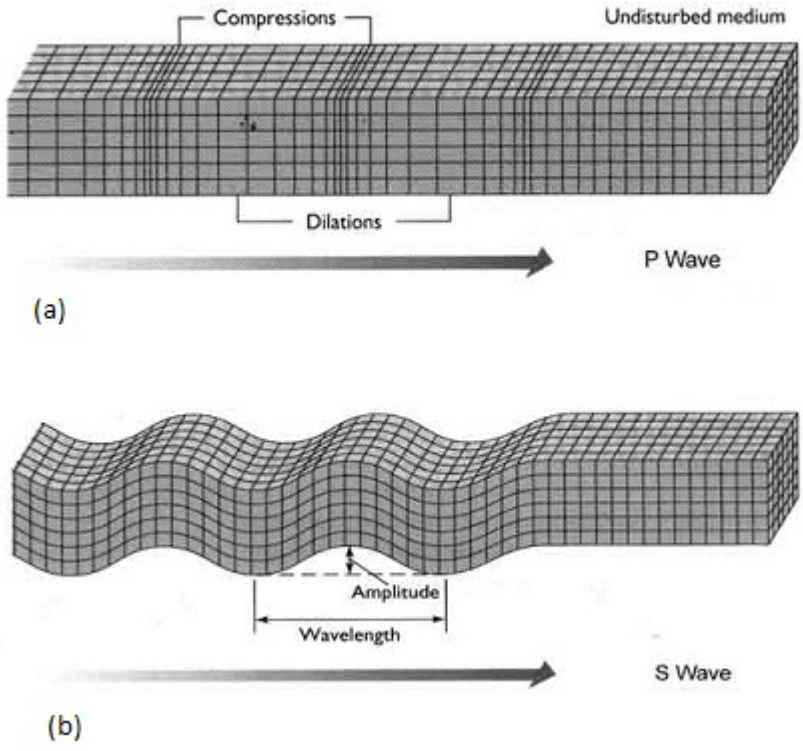

Figure 3-4: Diagram (a) represents the P- wave and (b) the S-waves (modified from Bruce A Bolt, Earthquakes).

When seismic waves are used to map earth structure, major task is to identify those parts of the seismogram that are due to the elastic response of the earth. When a seismometer detects and records seismic energy from an event such as a distant earthquake, the record is usually characterized by a number of distinct peaks which indicate the arrival of different phases. These phases represent different types of waves that propagate in an elastic medium (P-wave, S-wave, Love wave, Rayleigh wave) and the interactions of the source waveform with the material through which it propagates. Figure 3-5 shows an example of a distant earthquake record with several phases identified. Receivers placed at varying distances from a source will record phase arrivals at different times. If records are positioned side by side according to distance from the source, then coherent phases will form travel time curves whose geometries are dependent on subsurface velocity structure. This type of display is widely used in seismology because it helps identify different phases and gives an insight into subsurface structure.

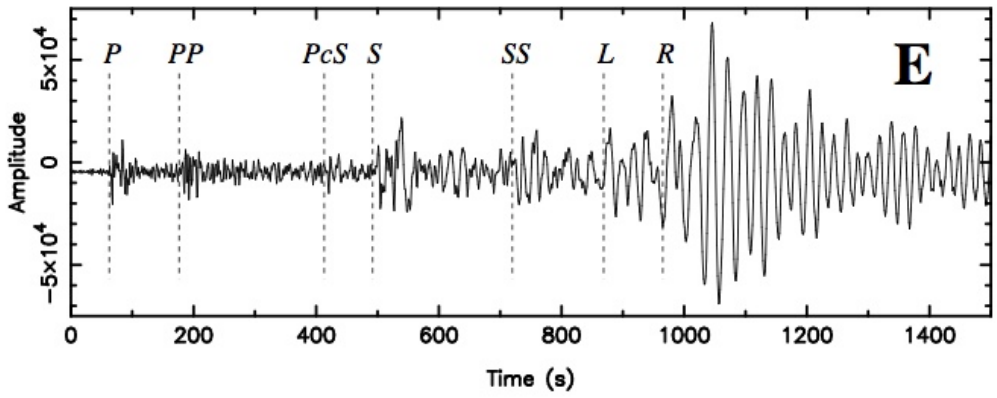

Figure 3-5: E-W component of a seismic waveform recorded in Shanghai, China from magnitude 6.7 earthquakes in the New Britain Region, PNG on 6th February 2000. Seven readily identifiable phases are picked. The angular distance between the earthquake source and receiver is 46°.

3.1.2 Receiver Function Technique

According to ray theory and the stress-strain boundary conditions that apply at welded boundaries, a wave field interacts with a boundary by partitioning into both transmitted and reflected waves of various polarization following conditions specified by the Zoeppritz equations (Aki and Richards, 2002). When a P –wave encounters an interface Figure 3-6(b) it transmits some energy through, including the Ps converted phase (also known as the vertical A wave component or SV). Ps conversion is advantageous because it arrives relatively early in the seismic record which prevents it from being lost among the many later arriving phases. A broadband sensor record data along three separate axes and so some processing is necessary prior to deconvolution in order to separate the incident and the converted wave phases. The simplest of these techniques involves recasting the seismometer traces into three orthogonal components which are radial, transverse, and the vertical directions (Rondney, 2009).

The P phase is estimated to remain confined on the vertical component of the seismogram while the converted Ps contribution is on the radial component in isotropic media, which is referred as horizontal component. The source wavelet, usually distance earthquake, is not known and must be estimated from the available seismogram. The P-wave component is used as an approximation of the source

wavelet because it is relatively unaffected by discontinuities, and Ps phase is used as recorded trace (Bostok, 1999). More sophisticated techniques of isolating the source wavelet and the trace minimize signal leakage between components of the seismogram by rotating the components into the direction of polarization of the incident wave field (Langston 1979)

The first –order information about the crustal structure under a station can be derived from the radial receiver function which is dominated by P-to-S converted energy from a series of velocity discontinuities in the crust and upper mantle. Because of large velocity contrast at the crust-mantle boundary, the Moho P-to–S conversion (p_S) is often the largest signal following the direct P in idealized case both the primary converted phases P_S and its multiples P_PP_S and $P_PP_S+P_SP_S$ are clear and have comparable amplitudes. Naming of these phases follows the convention of Bath and Steffannon (1966). By determining the difference in the arrival times of these phases and employing a velocity model, it is possible to estimate the depth of the discontinuity using the following equation:

$$H = t_{ps} / [(1 / Vs^2 - p^2)^{1/2} - (1 / Vp^2 - p^2)^{1/2}] \quad \ldots\ldots\ldots\ldots\ldots\ldots\ldots\ldots\ldots\ldots 2$$

Where H is the depth to the discontinuity, t_{ps} is the difference in time between the P arrival and the converted Ps phase, Vs is the S wave velocity, Vp is the P wave velocity, and p is the ray parameter (Al-Damegh et al., 2005).

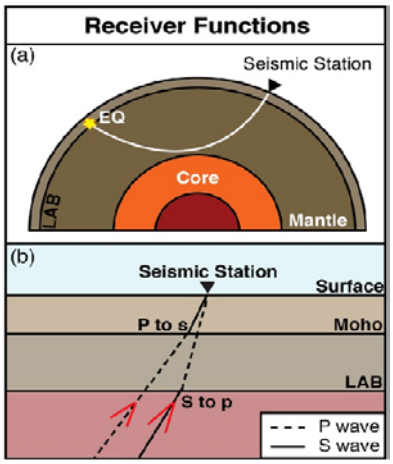

Figure 3-6 (a) Sketch cross-section of the Earth, showing hypothetical locations of a seismic station and a suitable seismic event for receiver function analysis. (b) At major velocity interfaces within the Earth, seismic waves may be converted from one phase to another as they cross the boundary from (Al-Damegh 2005).

Receiver function analysis is a straightforward simple method of extracting constraints on the crust and upper mantle structure from teleseismic waveforms recorded at three component seismic stations (Langston, 1979). A receiver function is a time series that, when convolved with the vertical component seismogram, reproduces the horizontal-component seismogram and the timing and amplitude of the arrivals in the receiver function are sensitive to the local earth structure (Langston, 1979). Langston (1979) pointed out that the basic characteristic of receiver functions, perhaps most impressive is the clean causal, seismogram like signal that results from the deconvolution of the vertical from the radial response of a plane layered structure. The simplicity of the method assures that it is a routine component of analyzing observations from a permanent network of stations and portable stations deployed as part of passive source temporary networks. Wide application of the technique has produced several complete descriptions of the receiver function methodology (e.g., Langston, 1979; Owens et ai., 1984; Ammon et al., 1990; Ammon, 1991).

The P wave receiver function (PRF) technique has been widely used to estimate Moho depths in various tectonic settings (Ammon, 1991; Kind and Vinnik, 1988; Langston, 1978; Yuan et al., 1997). In typical receiver function analyses, the Moho is associated with the significant seismic velocity contrast at the base of the crustal column, or more specifically, where the change in seismic velocity from ~6.5 km/s to greater than 8 km/s occurs over less than 1 km of vertical distance (Burdick and Langston, 1977).

Although the PRF technique can provide useful insight into crustal structures, the multiple P wave reverberations that follow the initial P arrival often mask the arrival of converted P to S phases. These reverberations make it difficult or impossible to identify deeper discontinuities such as the listhosphere-asthenosphere boundary (LAB). The use of converted S to P phase is used in this case, this because the converted S to P arrives earlier in the wave-train than the main S phase, S to P conversions are free of such reverberations, allowing identification of converted phases from deeper discontinuities and more complex structures (e.g. Kumar et al., 2007).

P wave receiver functions utilize teleseismic events occurring between 30° and 90° from the station. Beyond this range, incident rays do not arrive at angles steep enough

for conversion or the converted phases may be overprinted by surface reflections and reverberations. S wave receiver functions utilize events that are between 55° and 85° distant. For SRFs, events closer than ~55° are excluded as phases converted at the lithosphere-asthenosphere boundary are not observable due to over- critical incidence (Yuan et al., 2006). Beyond ~90°, SKS phases arrive earlier than the main S-phase, obscuring the S to P conversion so that events with epicentral distances greater than ~90° must also be excluded (Yuan et al., 2006). The PRF method is well established and used as a routine method (Langston, 1977; Vinnik, 1977). It is principally composed of two steps: coordinate rotation isolates the P- to-S converted waves from the P wave; and deconvolution removes the source-site complications and the propagation effects.

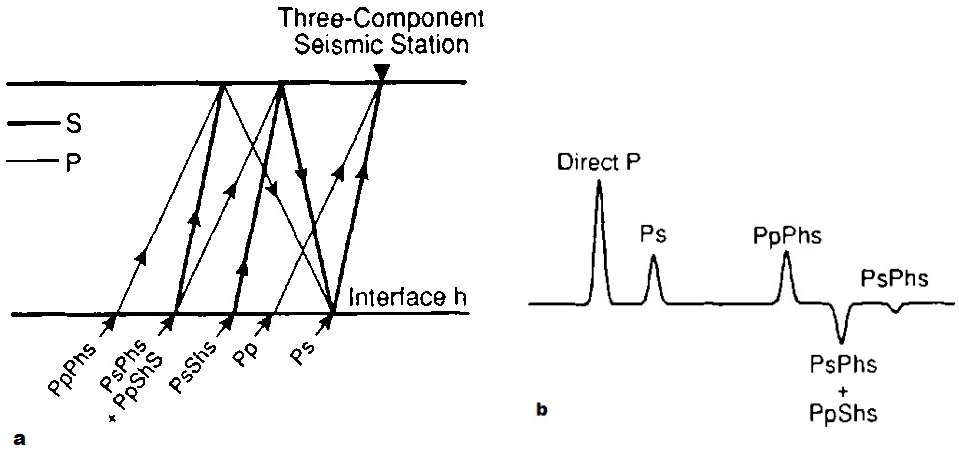

Figure 3-7: (a) Simplified schematics of a teleseismic earthquake arriving at a seismic station (Modified after Ammon, 1991).

Figure 3.7 (a) above, direct P-wave and waves that end as S-waves at the seismic station since the other P-waves are removed when creating the receiver function. Figure 3.7(b) is the corresponding simplified receiver function showing the converted P-waves at layer over a half space. Upper case letters indicate upgoing motion and lower case letters indicate downward motion. h indicates the reflection at the surface. For example PpPhs means an upgoing P-wave that is reflected in surface and bounce downward to the interface where it is reflected as an S-wave.

3.1.3 Processing and Calculating Receiver Function

To do the receiver function analysis two main steps are followed, these are Data rotation, Inversion (Deconvolution).

3.1.4 Rotation of Data

The two horizontal components N and E are rotated to radial (R) and tangential (T) directions. Most of the energy of the direct P and Ps waves are dominating the Z and R components, respectively. To isolate the converted Ps wave from the direct P wave, the ZRT components are rotated into an LQT (P-SV-SH) ray-based coordinate system, in which the L component is in the direction of the incident P wave; the Q component is perpendicular to the L component and is positive away from the source; the T component is the third component of the LQT right hand system. The L component is dominated by the P wave, while the Q and T components contain mainly the converted S wave energy. For horizontally layered homogeneous media, the converted S wave energy is exclusively contained in the Q component. Presence of significant energy in the T component indicates dipping and/or anisotropic structure.

However, a correct estimation of the incidence angle of arriving P wave is the main requirement to perform a perfect rotation. Overestimation or underestimation of the incidence angle can result in some P wave energy on the Q component of the receiver functions at the time of direct P wave (P-onset). Fortunately, these uncertainties only affect the observed delay times of the P-to-S conversions from very shallow conversions (the first 1-2 s).

The azimuth and incidence angle of incoming P waves can be either theoretically calculated or actually measured. Theoretical back azimuth and incidence angle are calculated from the locations of the recording station and the earthquake hypocenter, and are usually used in the case of low signal-to-noise P wave signals. If the incidence angle and azimuth of the incoming P wave are correctly estimated and the conversion phases do not originate from discontinuities dipping more than 10° (Langston, 1977), the isolating of the SV energy in the P coda is achieved and there will be no P wave energy left on the Q and T components. Moreover, since the first onset on the Q component is the converted Ps phase from a shallow discontinuity below the surface, it is theoretically possible to detect discontinuities even at shallower depth (sediment layer) in contrast to the radial component where the direct P arrival usually covers Ps conversions from very shallow reflectors.

3.2 Inverse Problem

In seismology a known incident wave is given and it's perturbed by a variation of the nominal features of the medium, if these variations are known, the calculation of the perturbation undergone by the incident wave (forward problem) represent a classic methods. Reciprocally, the measure of the perturbation of signal (seismograms) provides the supplementary data permitting reconstruction of an unknown variation of the nominal features (inverse problem).

In general inverse problems are hard to solve, we need to be concerned with far more than simply finding mathematically acceptable answers to parameter estimation, One reason is that there may be many models that adequately fit the data, and the process of computing an inverse solution can be, and often is, extremely unstable in that a small change in measurement then can lead to an enormous change in the estimated model. From the mathematical point of view we can represent many physical experiments with a model space consisting of model parameters $m_1 = (m_1 \ldots\ldots m_m)$ and a data space with data $d_1 = (d_1 \ldots\ldots d_n)$. Both the model parameters and the data are physical magnitudes whose functional relationships are given by a set of computational rules (the function f). If we assume that the fundamental physics are adequately understood, so a function may be specified relating and as

$$d = f(m) \ldots\ldots 3$$

Inverse problem cannot solve the system exactly, but have to minimize the misfit between data and model parameter m. Generally formulated, the data $d_1 = (d_1 \ldots\ldots d_n)$ are a series of observations in the form of measured values, whereas the model parameters $m_1 = (m_1 \ldots\ldots m_m)$ stand for the physical properties of the research object. The latter are not necessarily directly measurable. The function stands for a method (usually a mathematical representation of a physical theory), which relate the model parameters to data.

If the model parameters are given and the accompanying data calculated, then we speak of a forward problem (unique solution), on the other hand if we want to determine unknown model parameters based on the data (for example, physical measurements, then we speak of the inverse problem (not unique solution).

3.2.1 Deconvolution

To eliminate the influence of the source and ray path, an equalization procedure is applied by deconvolving the Q and T component seismograms with the P signal on the L component (Yuan et al., 2000, 2002). The resulting Q component data are named P receiver functions and are mainly composed of the P-to-S converted energy and contain information on the structure beneath a seismic station. The arrival time of the converted Ps phase in receiver functions depends on depth of the discontinuity, whereas the amplitude of the converted phase depends on the S-wave velocity contrast across the discontinuity.

The earliest receiver function studies such as Phinney (1964) worked in the frequency domain using the ratio of amplitude spectra to estimate the gross characteristics of structure. Langston (1979) extended the method to include phase information by using a complex frequency-domain ratio and inverse transforming back into the time domain. For his deconvolution he used a water-level stabilization method and a low-pass Gaussian filter to remove high-frequency noise not filtered by the water-level. There are three main methods of Deconvolution. These are Spectral Division: water level technique (Burdick and Langston, 1977), Frequency-Domain Deconvolution (Logoria and Ammon, 1999), Individual Iterative Time Domain Deconvolution (Ligoria and Ammon, 1999).

3.2.1.1 Water-level Deconvolution

In water-level deconvolution, the way we avoid division by small numbers is to replace small values in the denominator with a fraction of the maximum value (for all frequencies) value of the denominator. The fraction is called the water-level parameter (the water-level is the fraction multiplied by the maximum denominator amplitude), and is chosen by trial and error. The consequence of replacing small values with larger values in the denominator is an attenuation of frequencies for which the vertical component has small amplitude. At times the water-level can act as a high-pass, low-pass, and notch filter Ammon (2006).

The appropriate water level fraction is controlled by the signal-to-noise ratio and the nature of the vertical component seismogram and is chosen by examining the results of several trials water-level fractions and is choosing the lowest water –level that produces acceptable noise levels in the corresponding receiver function.

The deconvolution program requests a phase shift for the result. The phase shift moves the start of the receiver function from zero (the beginning of the time series) to the value you input. If you have "padded" the seismograms with noise or zeros before the deconvolution, you can shift the signal 30 seconds or so, and thus have a segment of the receiver function that under ideal circumstances should be zero. That part of the trace can be used to assess the level of processing noise in the receiver function.

3.2.1.2 Frequency-Domain Deconvolution

Let w represent angular frequency (2*pi*f), Z(w) and R(w) represent the Fourier transforms of the vertical, radial components of motion, and E_R(w) the Fourier transform of the radial receiver function. The receiver function is defined by

R (w) Z*(w) / Z (w) Z*(w)……..4

Z*(w) represents the complex conjugate of Z (w). A similar equation can be written for the tangential component of motion, defining the tangential receiver function.

To simplify the result, Langston (1979) introduced a low-pass Gaussian filter, G (w) into the procedure. The Gaussian was chosen because of its simple shape, zero phase distortion, and lack of side-lobes.

[R (w) Z*(w) / Z (w) Z*(w)] …….5

While the above equation is the definition of a receiver function, it cannot be used to compute observed seismograms because small or zero values of Z (w) Z*(w) cause numerical problems in the calculation. There are several approaches to avoid this problem, the simplest is the ad hoc approach called water-level deconvolution. This was the approach adopted by Langston (1979) and is still a very good method when the data quality is good. Other approaches such as time-domain inversion of the algebraic convolution equations are available, but in each instance a parameter similar to the water-level parameter must be selected (damping value, truncation fraction, etc. (Ammon 1999).

3.2.1.3 Iterative Deconvolution

In receiver-function estimation, the foundation of the iterative deconvolution approach is a least-squares minimization of the difference between the observed horizontal seismogram and a predicted signal generated by the convolution of an iteratively updated spike train with the vertical-component seismogram. For this discussion, we will assume that we are estimating the radial receiver function, but the approach is equally applicable to the transverse motion and can be easily generalized to accommodate simultaneous deconvolution of any number of signals. First, the vertical component is cross-correlated with the radial component to estimate the lag of the first and largest spike in the receiver function (the optimal time is that of the largest peak the absolute sense in the cross-correlation signal). The spike amplitude is estimated by solving a simple equation listed in Kikuchi and Kanamori (1982). Then the convolution of the current estimate of the receiver function with the vertical-component seismogram is subtracted from the radial-component seismogram, and the procedure is repeated to estimate other spike lags and amplitudes. With each additional spike in the receiver function, the misfit between the vertical and receiver-function convolution and the radial-component seismogram is reduced, and the iteration halts when the reduction in misfit with additional spikes becomes insignificant. This iterative deconvolution is used in this work.

3.3 The Gaussian Filter

The receiver function is smoothed with a Gaussian filter G (t) in order to eliminate high frequency errors introduced during the deconvolution. The smoothed receiver function waveform can be directly interpreted by visual inspection.

The Gaussian filter (Equation 6) is applied to the data before the calculation of the receiver function and is a very gentle low pass filter with no phase distortion and a simple shape (Langston, 1979; Ammon, 1997). It has one parameter, the width **a**, that controls the frequency response. The choice made for this filter effects the receiver functions and so can have an effect on the results of the Hκ stacking. In general, a smaller Gaussian removes the higher frequencies, and results in mostly longer periods in the receiver function. These longer periods are less affected by gradient boundaries as they tend to see them as steps in velocity, but there is a corresponding loss of resolution, particularly in Vp/Vs. The higher Gaussians tend to have much better resolution, but have less sensitivity to gradational boundaries and can have more trouble with noise.

$$G(w) = e^{(-w^2/(4a^2))} \quad \text{……..6}$$

Prior studies have made different choices for the Gaussian width a, and it is important to recognize that the results can vary with this choice. Zhu and Kanamori (2000) used a Gaussian width of 5.0 while Gilbert and Sheehan (2004) used 2.0 and Li et al. (2002) used 1.0.

3.4 Calculating the Receiver Functions

The earth's response to an incoming wave on a one-dimensional velocity structure is illustrated in figure 3-8, and it can be written as two components of motion as described by Ammon (1991). The vertical motion Z (t) and the radial motion R (t) can be written as:

$$R(t) = \sum_{k=0}^{n} r_k s(t - t_k) \quad \text{……7}$$

$$z(t) = \sum_{k=0}^{n} Z_k S(t - t_k) \quad \text{……8}$$

Where s (t) is the source signal time function, z_k and r_k are the amplitudes of k'th ray on each component, t_k is the arrival time of the k'th ray at the surface. The sums are over n rays with k = 0 being the direct P-wave.

Assuming that s $(t - t_k)$ is a delta function the Fourier transforms can be written as

$$R(w) = r_o \sum_{k=0}^{n} \hat{r}_k \, e^{-i\omega t_k} \quad \text{.....9}$$

$$Z(w) = z_0 \sum_{k=0}^{n} \hat{z}_k \, e^{-i\omega t_k} \quad \text{.....10}$$

Where Z(t) and R(t) are the vertical and radial component respectively, s(t) is the source time function and tk is the arrival time of the k'th ray with the sum over n being the sum of n rays, and zk and rk being arrival of the kth ray for each component. The deconvolution of the vertical motion from the radial can be written as

$$H(\omega) = \frac{S(\omega)R(\omega)}{S(\omega)Z(\omega)} = \frac{R(\omega)}{Z(\omega)} \quad \text{.....11}$$

R(ω) in frequency domain yields the Fourier transform of the receiver function H(ω). The source spectrum S (ω) is cancelled out through this process Ammon (1991).

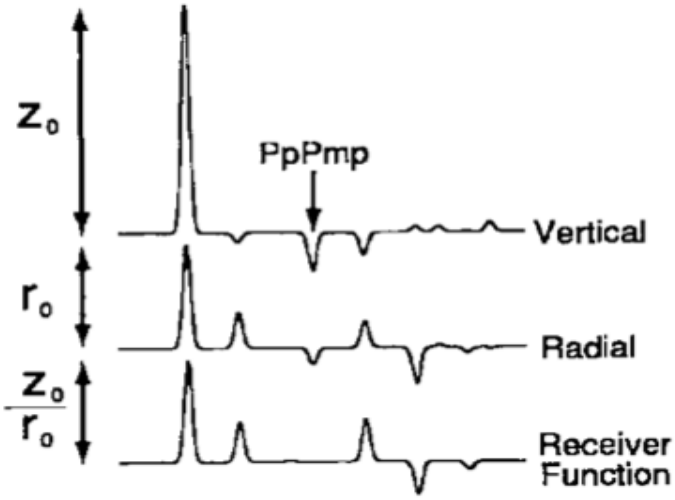

Figure 3-8: The vertical and radial response to an incoming signal and the resulting receiver function. Notice that the PpPmp wave is not present in the receiver function (Ammon, 1991).

The example is presented here where a plane wave arrives underneath a seismic station. The three distinct arrivals on the seismic station are the direct P-wave, a P-wave reflected at the interface and finally a P-wave that have been converted into S-wave at the interface. When a P-wave impinges on a boundary to a layer with a different seismic velocity the wave will be reflected and refracted in the boundary. If the layer is not fluid a secondary S-wave will be generated, (Lay and Wallace, 1995,). For teleseismic waves the converted S-wave is much stronger in the horizontal component than in the vertical component of the recorded data. This difference in strength of signal in the horizontal and the vertical components form the core of the method.

The Fourier transform of the motion in the radial and vertical direction from the three arrivals can be written as:-

$$E_R(\omega) = r_0\left[1 + \hat{r}_p e^{-i\omega t_p} + \hat{r}_{ps} e^{-i\omega t_{ps}}\right] \quad \text{.....12}$$

$$E_z(\omega) = z_0\left[1 + \hat{z}_p e^{-i\omega t_p} + \hat{z}_{ps} e^{-i\omega t_{ps}}\right] \quad \text{.....13}$$

The first term inside the parenthesis corresponds to the direct P-wave, the second term corresponds to the reflected P-wave and the final term corresponds to the S-wave. The main part of S-wave energy is given in the horizontal component hence it is clear that, $\hat{Z}_{ps}$, the amplitude of the S-wave relative to the amplitude of the direct P-wave, must be much less than one $\hat{Z}_{Ps} \ll 1$. Thus using equation 11, 12 and 13 we get the following equation:

$$H(\omega) = \frac{r_0}{z_0} \frac{1 + \hat{r}_p e^{-i\omega t_p} + \hat{r}_{ps} e^{-i\omega t_{ps}}}{1 + \hat{z}_p e^{-i\omega t_p}} \quad \text{.....14}$$

For a plane wave arriving at a horizontal interface the rays are parallel and $\hat{r}_p = \hat{Z}_p$

$$H(\omega) = \frac{ro}{zo} \frac{1 + \hat{z}_p e^{-i\omega tp} + \hat{r}_{p_s} e^{-i\omega tps}}{1 + \hat{z}_p e^{-i\omega tp}} \quad \text{.....15}$$

Using the binomial expansion: $(1+x)^{-1} = 1 - x + x^2 + \ldots$

$$H(\omega) \cong \frac{r_0}{z_0}\left(1 - \hat{z}_p e^{-i\omega t_p}\right)\left(1 + \hat{r}_p e^{-i\omega t_p} + \hat{r}_{ps} e^{-i\omega t_{ps}}\right) \quad \ldots 16$$

=

$$\frac{r_0}{z_0}\left(1 - \hat{z}_p e^{-i\omega t_p} - \hat{z}_p\,\hat{r}_p e^{-2i\omega t_p} - \hat{z}_p\,\hat{r}_{ps} e^{-i\omega(t_p + t_{ps})} + \hat{r}_p e^{-i\omega t_p} + \hat{r}_{ps} e^{-i\omega t_{ps}}\right) \quad \ldots\ldots 17$$

Neglecting higher order terms

$$= \frac{r_0}{z_0}\left(1 - \hat{z}_p e^{-i\omega t_p} + \hat{r}_p e^{-i\omega t_p} + \hat{r}_{ps} e^{-i\omega t_{ps}}\right) \quad \ldots\ldots\ldots 18$$

Plane wave means $\hat{Z}_p = \hat{r}_p$

$\therefore$

$$H(\omega) = \frac{r_0}{z_0} + r_{ps} e^{-i\omega t_{ps}} \quad \ldots\ldots\ldots 19$$

↑ ↑

P- Wave P_S- Wave

Figure 3-6 an example of synthetic receiver functions showing the direct P, the converted P_S and the multiples.

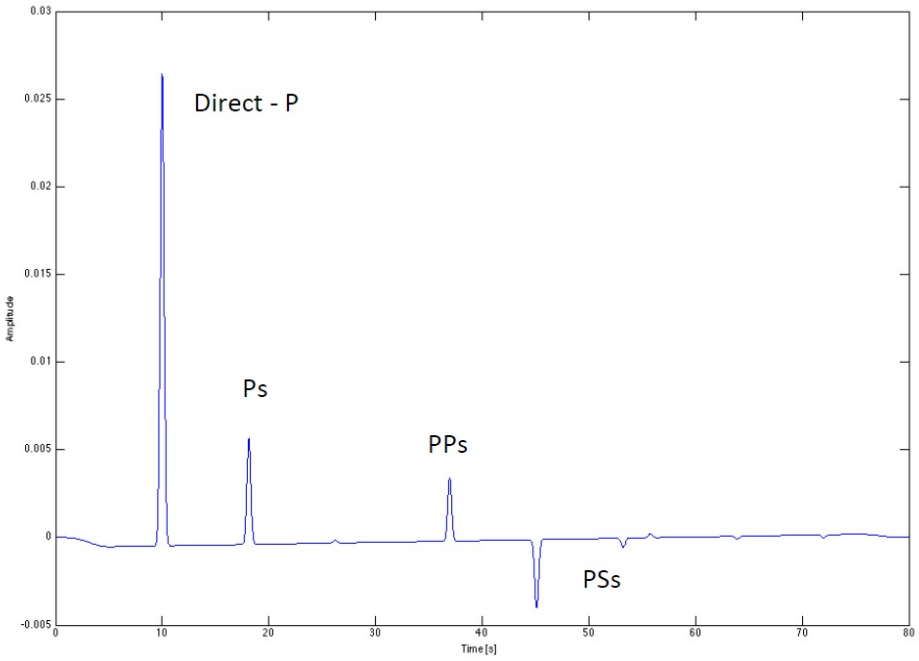

Figure 3-9: Synthetic receiver function the direct-P, Ps, PPs, and PSs phases are labeled.

3.5 Inversion to Extract the Velocity Structure from Receiver Function

3.5.1 DEPTH CONVERSION

The first order information about the crustal structure under a station can be derived from the radial receiver function which is dominated by P-to –S converted energies from a series of velocity discontinuities in the crust and upper mantle. Because of the large velocity contrast at the crust-mantle boundary, the Moho P-to –S conversion (p_s) is often the largest signal following the direct P.

The time separation between P_S and P can be used to estimate crustal thickness, given the average crustal velocities

$$H = \frac{t_{Ps}}{\sqrt{\frac{1}{V_S^2} - p^2} - \sqrt{\frac{1}{V_P^2} - p^2}},$$

…….20

The equation relates the delay time of a *Ps* phase, *tPs*, to the depth at which the conversion took place, H, where V_P and V_S are the average *P*- and *S*-wave velocities above the depth of the conversion and *p* is the ray parameter (Zhu & Kanamori 2000).An advantage of this method is that because p-to-s conversion point is close to the station, the estimation is less affected by lateral velocity variation and thus provides a good point measurement. One problem is the trade-off between the thickness and crustal velocities. However since tP_S represents the differential travel time of S with respect to P wave in the crust, the dependence of H on V_P is not as strong as on V_S (Zhu & Kanamori 2000).

3.5.2 LINEARIZED TIME DOMAIN WAVEFORM INVERSION

Our problem is to translate the information contained in the receiver functions into a simplified model of the subsurface structure. The forward problem may be described by:-

$$d_j = F_j\,[m] \qquad j = 1, 2, 3,\text{-- } N \quad (1)\ldots\ldots\ldots\ldots\ldots\ldots 21$$

where d_j represents the N data points and F_j represents the functional which operates on the model m (an M-dimensional vector) to produce the waveform.

Throughout this discussion we represent vectors with boldface lowercase letters, matrices with boldface uppercase letters, and scalars with italics. The relationship (21) is nonlinear and for waveform inversions represents the numerical calculation of synthetic seismograms Ammon et al. (1990). We parameterize the velocity structures as M-dimensional vectors of shear wave velocities and keep the layer thicknesses fixed. We begin the solution for an estimate of the true velocity model, m, with an initial approximation to the local receiver structure, represented by the vector of layer velocities $M_{0.}$ Initial guesses are usually developed using the results of earlier geophysical investigation of the region or similar regions. An important assumption of the time domain inversion scheme is that the initial model $M_{0,}$ is close to the true earth velocity structure M, Ammon et al. (1990). Under such conditions the problem may be linearized by expanding the observed receiver function in a Taylor series about m_o

$$F_j\,[m] = F_j\,[mo] + (D, \delta m)_j + O||(\delta m^2)||\ldots\ldots\ldots\ldots\ldots\ldots 22$$

Where (D, δm) represents the inner product between the matrix D, which is the partial derivative matrix of the functional F_j at m_0, and the model correction vector, δm . Discarding the nonlinear terms $O||(\delta m^2)||$ complete the linearization

The inversion scheme developed by Ammon et al. (1990) is based on the "jumping" version of the iterative LSQ solution:

• Creeping

$d = F(m)$

$d = F(m0) + \nabla F|m0\ (m-m0)$

$\delta y = \nabla F|m0\ \delta m$ …….23

• Jumping

$d+\nabla F|m0\ m0 = F(m0)+\nabla F|m0\ m$

$\Delta d + \nabla F|m0\ m0 = \nabla F|m0\ m$ ……..24

• LSQ Norm

$E = ||\Delta d - \nabla F|m0\ (m - m0)\ ||2$ ……25

3.5.3 Over-parameterization & Regularization.

A frequent observation of receiver function inversions is a significant amount of rapid variation in the resulting velocity structures with depth. While there is no reason to assume the earth does not contain rapid velocity variations, many of the large-amplitude rapid variations in the resulting models may be due to under damping the receiver function inversion. In seismic studies where more than one model can always satisfy the data, the most important a priori constrain its consistency with independent geophysical and/or geologic information. An additional, subjective property of a preferred solution is simplicity. For this reason we implement smoothness constraint in our inversions by minimizing a model roughness norm [Constablee t al., 1987]. As shown in equation 26 below, minimizing the roughness of the model can trade-off with fitting more details in the waveform.

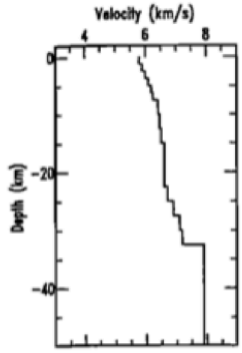

$$\begin{cases} \Delta \mathbf{d} + \nabla F\, \mathbf{m}_0 = \nabla F|_{m0}\, \mathbf{m} \\ \mathbf{0} = \sigma\, D\, \mathbf{m} \end{cases}$$

$$D\,\mathbf{m} = \begin{bmatrix} 1 & -2 & 1 & & \\ & 1 & -2 & 1 & \\ & & : & & \end{bmatrix} \begin{bmatrix} m_1 \\ m_2 \\ : \end{bmatrix}$$

$$E = \| \Delta \mathbf{d} - \nabla F\, (\mathbf{m}-\mathbf{m}_0) \|^2 + \sigma^2 \| D\mathbf{m} \|^2 \qquad \text{……..26}$$

3.5.4 Choosing the Smoothness Parameter

Ps phase from the crust-mantle transition region, which is less sensitive to the sharpness of the boundary, is well modeled by the smoother models. Figure 3-10 characterizes the waveform fit, model smoothness trade-off by comparing model roughness with the rms residual of the waveform fit. Model roughness is measured by summing the absolute amplitude of the velocity difference normalized by the number of layers used to compute the difference (second difference in this study) throughout the model. For example, a second difference roughness calculation is described by (Ammon et al 1990)

$$\text{roughness} = \sum_{i=1}^{n-2} \frac{|\alpha_i - 2\alpha_{i+1} + \alpha_{i+2}|}{(n-2)} \qquad \text{……27}$$

where a_i is the P wave velocity of the *i*th layer and n is the total number of layers in the velocity model. Note that in Figure 3-10 the minimum in rms fit does not correspond to the roughest model. However, this minimum in the rms is not well defined. The choice of the smoothness parameter is somewhat subjective, although with real data, a useful criterion for the smoothness trade-off parameter is to find the value which produces an rms error approximately equal to the rms of presignal noise in the receiver function stack (Ammon et al 1990).

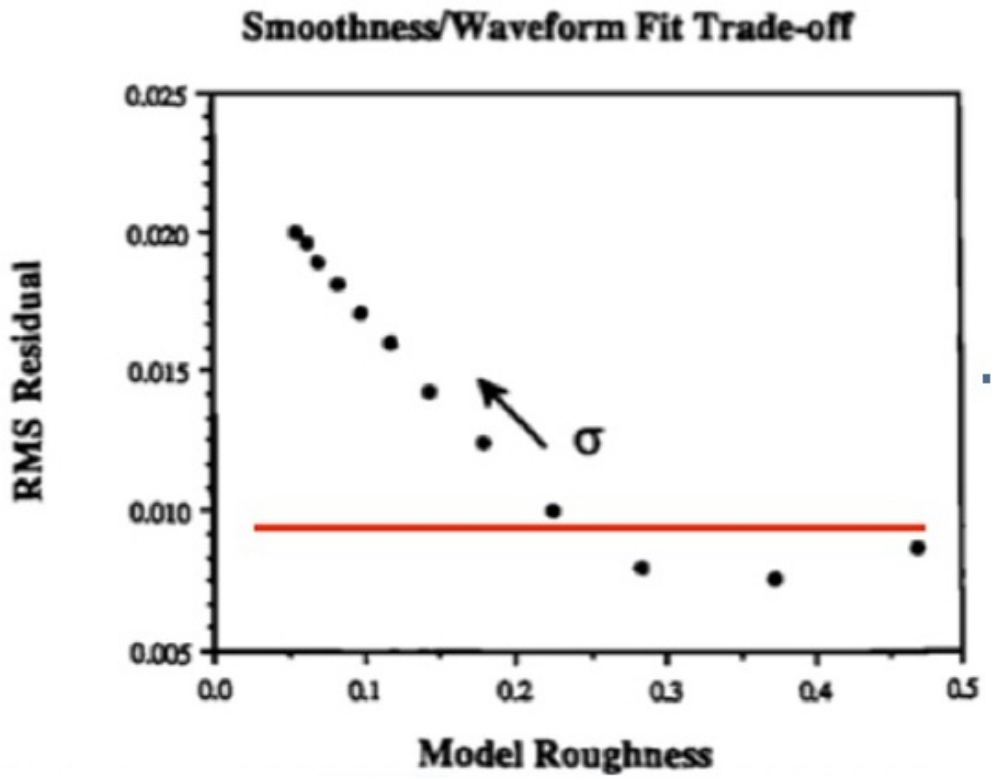

Figure 3-10 Smoothness/waveform fit trade-off for the 12 inversion with varying smoothness trade-off parameter. As trade-off parameter increases, the model roughness decreases and the length of residual vector increases A value for σ is chosen, for instance, from the noise level from the transverse RF(from Ammon et al 1990).

3.5.5 The Non-Uniqueness Problem

Ammon et al. (1990) showed that the modeling of receiver function waveforms is non-unique as in figure 3-11.

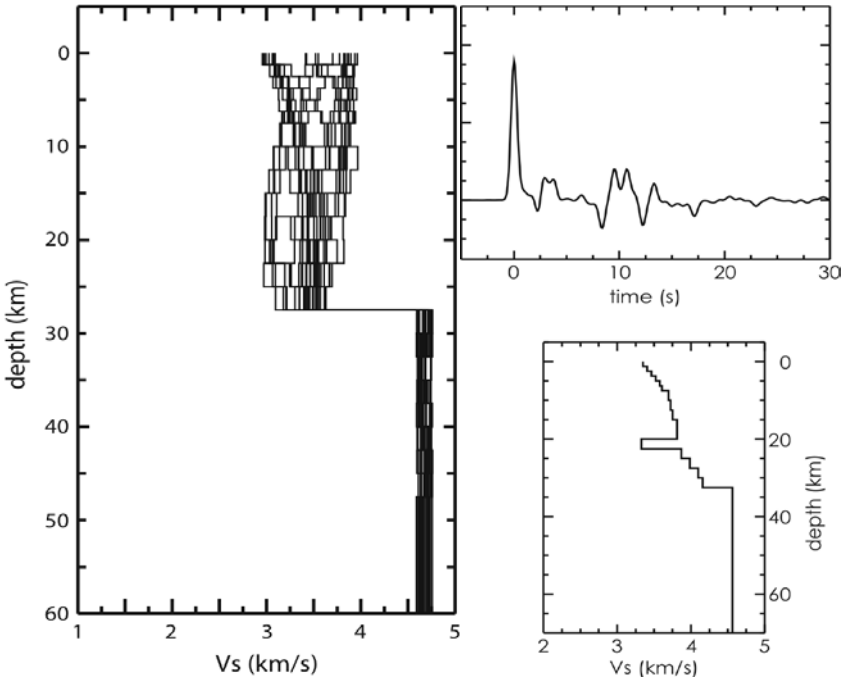

Figure 3-11: The figure above show the modeled velocity of Vs (km/s) versus the depth and also the receiver function Ammon (1990).

3.6 Summarizing:

The following summary of inversion scheme proposed by Ammon et al. (1990) for the modeling of receiver functions is:

1) Construct an initial model with a stack of many thin layers
2) Determine the smoothness parameter through a “preliminary” inversion.
3) Investigate the multiplicity of solutions by perturbing the initial model into many starting models.
4) Choose a model from a priori and independent information

CHAPTER FOUR

4.0 Data Acquisition and Analysis

4.0.1 Introduction

The teleseismic data used in this research was recorded by Lodwar seismic station. The station is permanent seismic station and is part of GEOFON network funded by GeoForschungsZentrum (GFZ), Potsdam, Germany in collaboration with the University of Nairobi and the Kenya Meteorological Department. The station operates under SEISCOMP3 software. The data used in this study was collected for a period of one year from 1st January 2012 to 31st December 2012. The data was analysed and plotted on the Global map figure 4-1. The data used is in plotting the map is in appendix 12

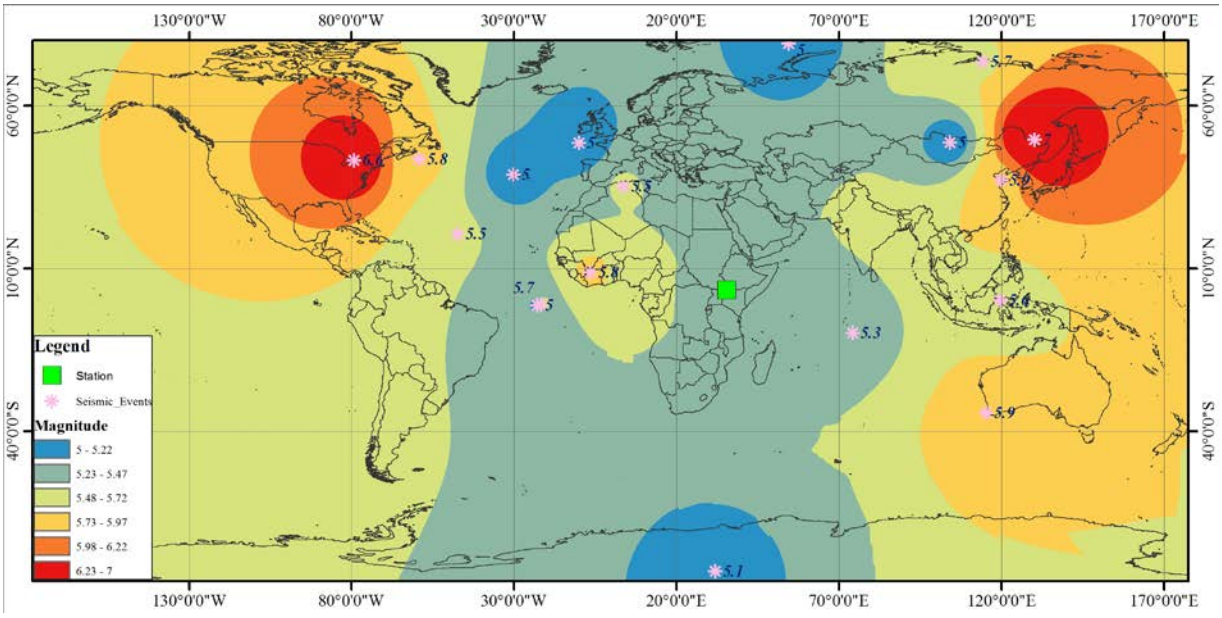

Figure 4-1: Teleseismic event used in receiver function analysis plotted on the global map.

4.1 SeisComP3 software and data acquisition

SeisComP is likely the most widely distributed software package for seismological data acquisition and real-time data exchange over the internet. Its data transmission protocol SeedLink became a de facto world standard. The first version of SeisComP was developed for the GEOFON network and further extended within the MEREDIAN project under the lead of GEOFON/GFZ Potsdam and ORFEUS.

Originally SeisComP was designed as a high standard fully automatic data acquisition and (near-) real-time data processing tool including quality control, event detection and location as well as dissemination of event alerts. In the context of the GITEWS project (German Indian Ocean Tsunami Early Warning System) additional functionality were implemented to fulfill the requirements of 24/7 early warning control centers. Major changes in the architecture of SeisComP were necessary and many new features result in the upgrade of SeisComP to version 3.0. SeisComP3 provides the following features:

- Data acquisition
- Data quality control
- Data recording
- Real-time data exchange
- Network status monitoring
- Real-time data processing
- Issuing event alerts
- Waveform archiving
- Waveform data distribution
- Automatic event detection and location
- Interactive event detection and location
- Event parameter archiving
    - Easy access to relevant information about stations, waveforms and recent earthquakes (Trabant and Heinloo, 2004)

The new requirements for early warning purposes made it necessary to adapt the design and architecture of the previous SeisComP. The guidelines for the design of SeisComp3 are:

- Implementation of critical functions as standalone modules to guarantee the independence from other functions (e.g. picker, magnitude calculation, interactive analysis)

- Easy implementation of custom module

- Independence of hard- and software

- Ability of data exchange between different automatic real-time systems

- Distribution of modules on several systems

- Robust system for rapid and reliable earthquake solutions (especially during seismic crises)

4.2 SeedLink

SeedLink is real-time data acquisition protocol and client-server software that implements this protocol. The SeedLink protocol is based on TCP. All connections are initiated by the client. During handshaking phase the client can subscribe to specific stations and streams using simple commands in ASCII coding. When handshaking is completed, a stream of SeedLink "packets" consisting of a 8-byte SeedLink header (containing the sequence number) followed by a 512-byte Mini-SEED record, is sent to the client (Trabant and Heinloo, 2004).

The data is in mini-seed format and the channels are not combined but separate in different folder as shown below thus the need to merge the data so that you get three-channel stream in one window.

BH1.D BH2.D BHZ.D

4.3 Data Processing

The data from the station was read in the SEISAN software for ease of use, seiscomp3 software does support the analysis of the data but for this research SEISAN software was opted. The data was loaded in a computer installed with SEISAN 9.0 software and the database created. The procedure making a database is shown in the appendix 2. Then data was copied in the wor, wor is the working directory in SEISAN.

The command Dirf in SEISAN shows the numbered list of files corresponding to the file name & wildcards. The file is called ‘filenr.lis. it is placed in \wor\.

AUTOREG which generates and s-file for each waveform file was run, this process puts the s- files into the REA\LODK database for continuous data. NOTE: YOU MUST MANUALLY TRANSFER THE WAVEFORM FILES FROM \WOR TO THE APPROPRIATE \WAV DIRECTORY FOR THE DATA. Running the AUTOREG is shown in Appendix 3.

4.3.1 CREATING STATION0.HYP

The station HYP is stored in the DAT directory in SEISAN. The DAT directory contains station files, program parameters files with information about channels. Parameters used for spectral analysis are stored here as well as map contours (Havskov and Ottemoller 1999).

STATION0.HYP lists parameters used in the location program HYP appendix 4. There are many important parameters here to modify, including parameters for the

- Coda magnitude calculation,
- Station locations,
- Velocity model and
- Network code.

I. Coda duration magnitude parameters TEST(7), TEST(8) and TEST(9):

These parameters are the duration magnitude coefficients used for calculating the coda magnitude, as MAG = TEST (7) +TEST(8) * LOG(T) + TEST(9)* DELTA

Where T is the coda length in seconds,

DELTA is the hypocentral distance in km.

The default SEISAN values for the coda magnitude parameters are those

determined by Richter for Northern California.

Default values: 7: 0.087,

8: 2.0,

9: 0.0035 (Lee, 1972)

So default MAG = 0.087 +2.0 * LOG (T) + 0.0035 * DELTA

ii. Station locations:

Follow the format of the examples in STATION0.HYP for station location

iii. Velocity structure:

The velocity structure is given as shown in figure 4-2,

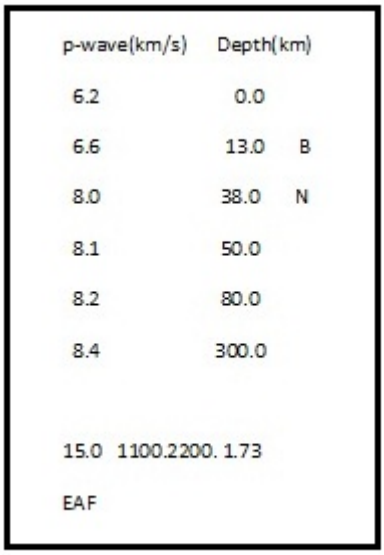

Figure 4-2: The model used showing the p-wave velocity (km) and the Depth to the Interface (from Eastern and Southern Seismological Working Group)

4.3.2 Data analysis in SEISAN using EEV

SEISAN is an interactive software where one is be able to easily jump from event to event and run several different programs with one event without restarting every time. This is done with the command EEV. In this interactive mode, events is picked, edited, located, moved, deleted, until satisfactory solution is found. EEV is designed to work with registered events in a specific database within a specific time, usually one month. Appendix 5 gives the several ways to start EEV.

4.3.3 Events processing using MULPLT

MULPLT is a general plotting and signal analysis program, this program is capable of doing general phase picking, correct for instrument response, and produce a wood-Anderson seismogram for determining Ml, traces for Mb and Ms, determine azimuth of arrival for 3 component stations, do spectral analysis and particle motion (Havskov and Ottemoller 1999). Figure 4-3 is a 3component MULPLT, MULPLT operates either in database independent program, in connection with database or using a continuous database started by command MULPLT.

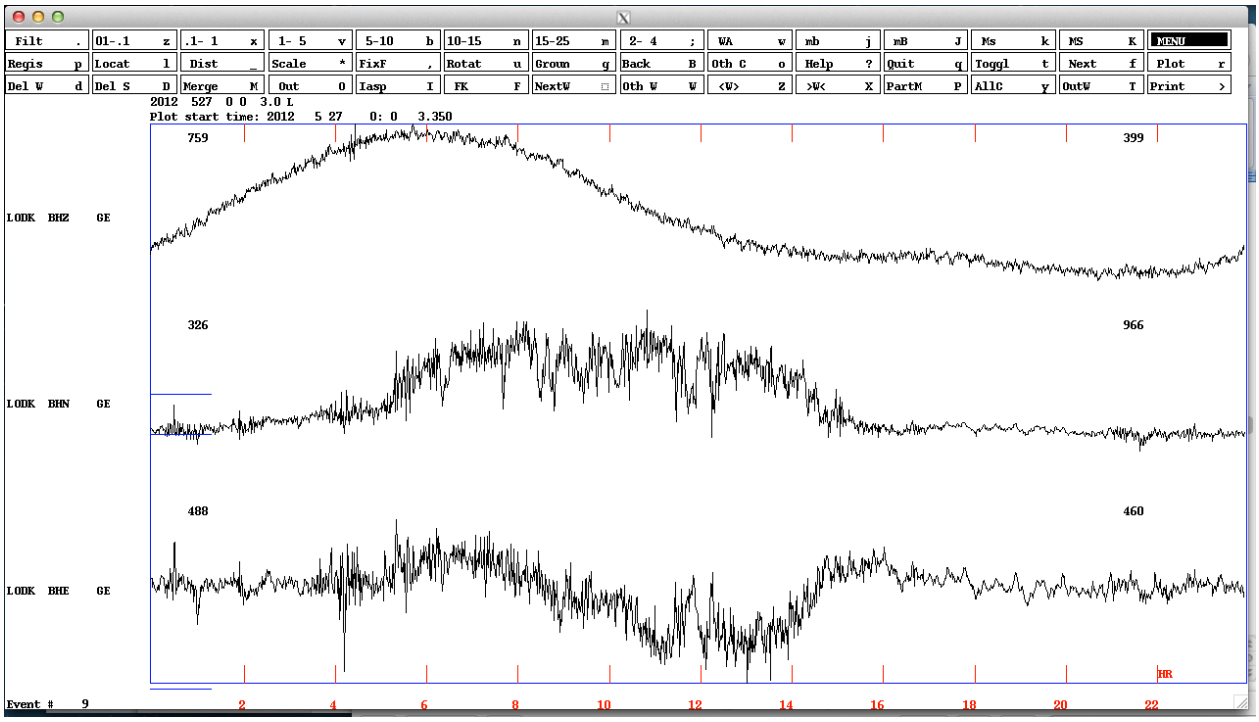

Figure 4-3: MULPLT screen in multi-trace mode.

4.3.4 Filtering the data

A filter of 01-0.1 Hz was used, without filtering nothing can be seen in the above broadband station. After filtering the window in figure 4-4 appears. SEISAN can filter one way pressing the key once or filter both ways by pressing filter key twice.

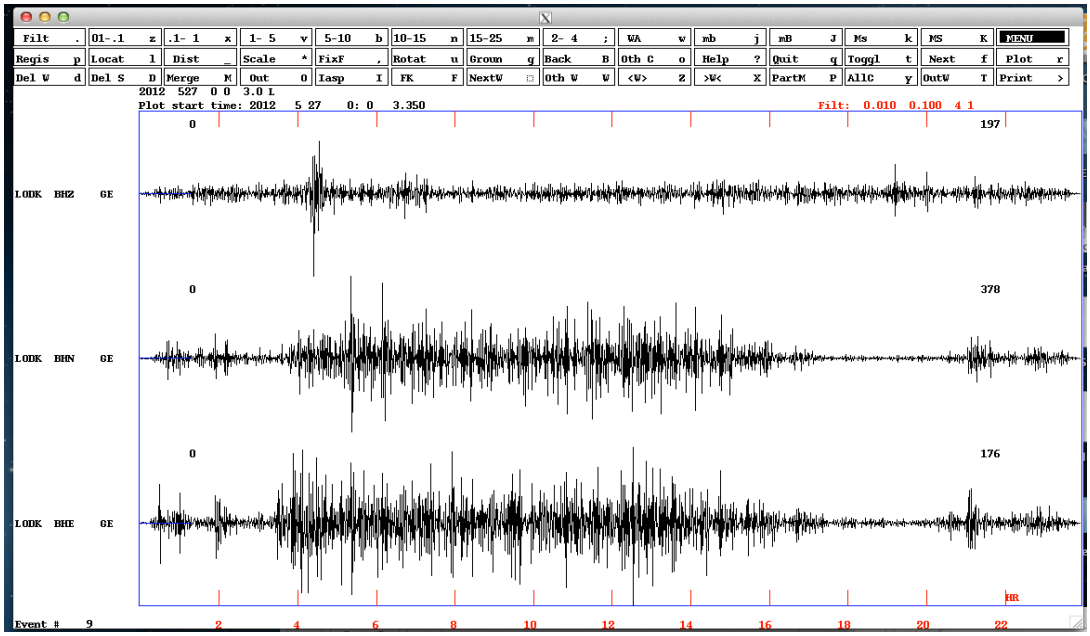

Figure 4-4: Screenshot of a 0.1Hz – 1z filtered data showing events recorded.

4.3.5 Viewing event spectrum:

The multitrace mode in MULPLT, Select the 'Toggle' button to toggle to single-trace mode, figure 4-5. From the single-trace mode in MULPLT,

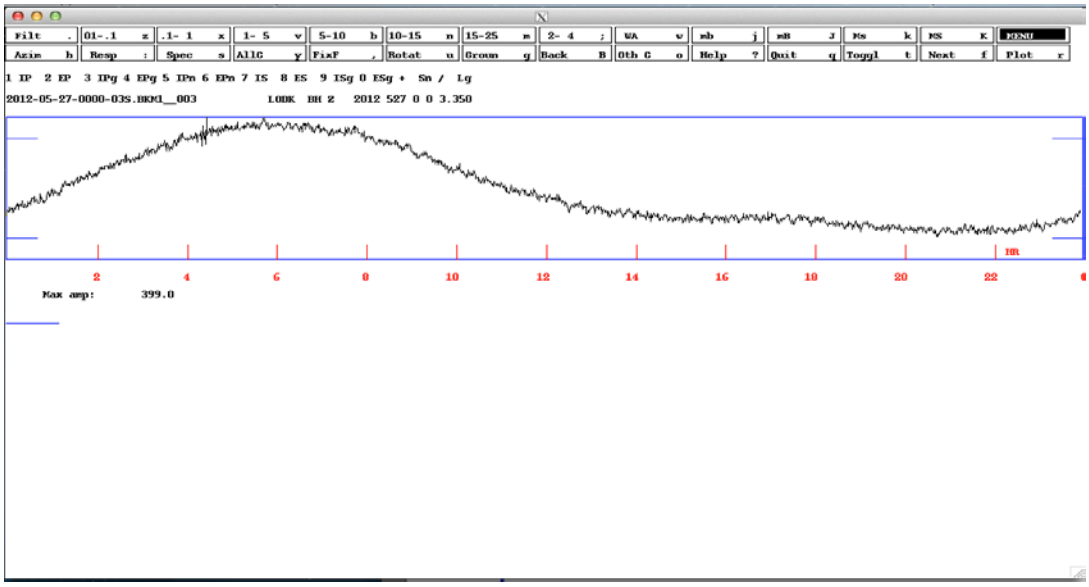

Figure 4-5: Mulplt showing a single trace where p wave and S-wave are picked

4.3.6 Event Location Using Single Station

Events were located using a single station, this because the data from other station within the country were not available. The procedure was done using the MULPLT,

this is a general plotting and signal analysis program in SEISAN. MULPLT permits the use of a single 3-comp station for event location. (For this capability to be implemented, the RESET TEST (56) variable in STATION0.HYP must be set =1, the default setting) In this technique, the p-arrival, s-arrival and back-azimuth are used to give a general location. The azimuth reading calculated by MULPLT is from the station back to the hypocenter, with reference to True North (not Magnetic North; note that many 3-comp sensors are oriented with respect to magnetic north. The local magnetic declination must be taken into account to get the true azimuth (Havskov and Ottemoller 1999). The procedure for locating the event is as follows-:

i) Select the p arrival.

ii) Display any one of the three components – if you picked the p-arrival on the z-component display that one.

iii) Select a time window around the p-arrival by clicking above the trace window figure 4-6. The window should be several seconds or tens of seconds before and after the p-arrival. If the 3-component is a broadband, select a filter first (Try the 01-1.0 filter).

iv) Select the 'Azim' button and select a zoom window around the p-arrival of a few tenths of second's duration.

v) The 3 components are now displayed in order along with calculated azimuth of arrival, apparent velocity and correlation co-efficient. Repeat this procedure a few times, experimenting with different window lengths and filters.

vi) The azimuth should be reasonable, and the correlation coefficient should be as high as possible and positive. Sometimes the correlation coefficient cannot be made positive, despite heroic efforts. The 'vel' (apparent velocity) will usually be unrealistic. To refresh the screen between attempts, select the 'plot' button.

vii) When you are satisfied with the azimuth, save it to the s-file by associating it with a phase. The usual way to do this is to pick an I or E phase (type 'e' or 'i'). That phase must be picked on the single upper trace seen on the same screen

viii) Return to multitrace mode by selecting the 'other c' button, and selecting the

‘all’ and ‘ok’ button for all the traces.

ix) Select the ‘Locat’ button to locate the event. The command screen appears as the location is calculated, and the results are written to the command window. The waveform plot shows both the manually-determined phases and the calculated phases.

x) If you are locating the event from secondary processing in EEV, after locating the event you must update the s-file to include the location by typing the ‘update’ command at the EEV command prompt. Update will run the location program again and write the results to the s- file.

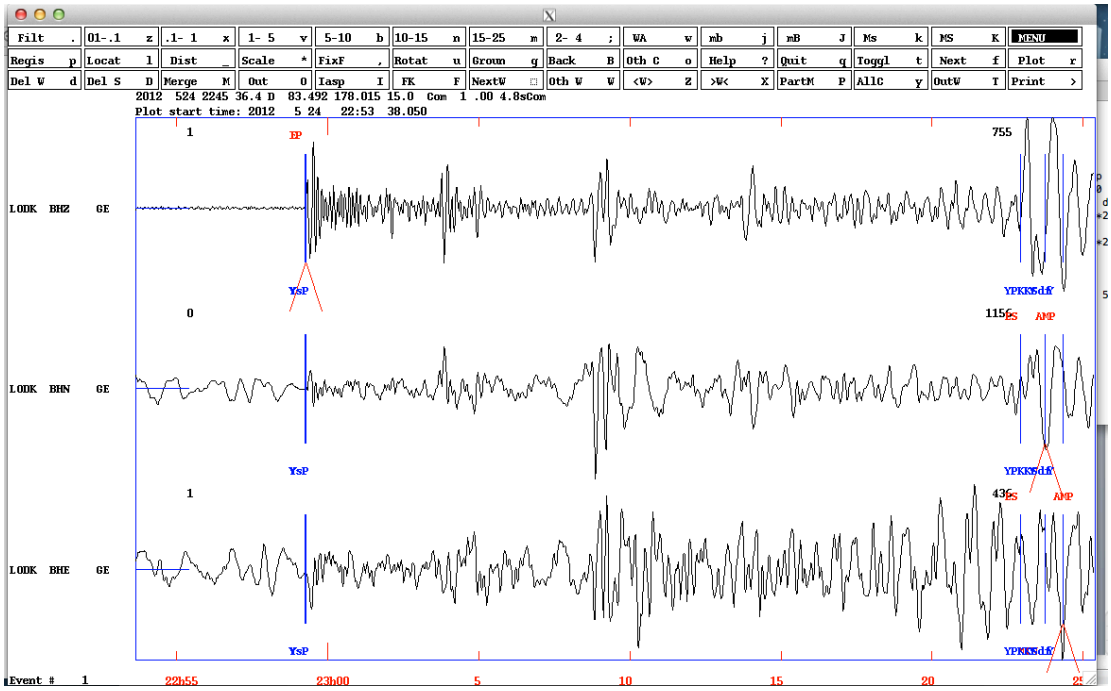

Figure 4-6: Mulplt of the multitrace screen showing manually-determined and calculated phases.

Here is a portion of the EEV terminal session showing the UPDATE process, type u and the following results will appear on your screen. The results show the station code, waveform file names, azimuth, epicentral distance etc. Figure 4-7 show an example of the updated file extracted from the data.

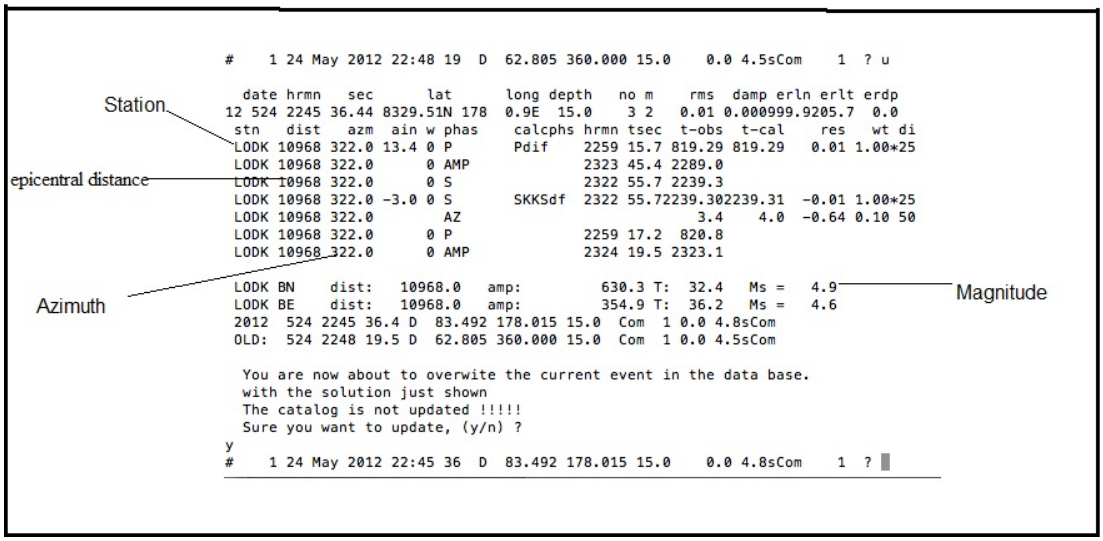

Figure 4-7: Updated event after analysis with EEV

4.3.7 Conversion of SEISAN Data To SAC

For receiver function analysis the data must be converted to SAC (Seismic Analysis Code) format appendix 1.Thus the data was converted from SEISAN to SAC format SAC is developed at Lawrence Livermore National Laboratory over the last 10-20 years. The main features of SAC include general arithmetic operations, Fourier transforms, three spectral estimation techniques, IIR and FIR filtering, signal stacking, decimation, interpolation, correlation, and seismic phase picking. SAC also contains an extensive graphics capability.

With SAC it is possible to write macros, which helps to process large amounts of data. The conversion process from SEISAN to SAC is illustrated in appendix 6. SAC contain headers, header in sac consist of important information about the data, such as the sampling interval, start time, length, station location, event location, components, phase arrivals, etc. There parameters are used by various SAC command to process the data. It is important to keep your header information complete and updated. An example of SAC header is show in appendix 11

4.4 Data Selection

I. Teleseismic events with epicentral with distance of 30° to 90° were selected to calculate receiver function. For measurements closer than 30°, the P-wave of the waveform is complicated by upper mantle travel path effects. On the other hand, if it is farther than 90°, the station is located within the shadow zone of the direct P-wave.

II. The earthquake (teleseismics) should have intermediate to large magnitudes (M > 5.5), with smaller magnitudes do not generate clear peaks and troughs in the waveforms.

III. The earthquake selected had depth that ranged from narrow, intermediate and deep.

A total number of 24 teleseismic events were located with magnitude ranging from 5.0 to 7.0.

4.5 Compilation of receiver function codes written by Charles Ammon in SAC (Seismic analysis code)

Receiver function codes written by Charles Ammon were used in this dissertation. The codes were in downloaded from the internet and compiled in the computer installed with SAC environment. The codes were unpacked using the command “zcat Rftn.Codes.Z | tar xvf-”. , compiled and installed.

4.6 Steps of carrying out receiver function

After the successful compilation of the codes in the computer, the following step were used to perform receiver function analysis

i) Data Preparation

ii) Source Equalization (Receiver-Function Estimation)

Deconvolution Programs

Frequency Domain

Time Domain

Iterative Deconvolution(iterdecon)

iii) Forward Modeling Programs

Creating a velocity model (icmod)

Computing a synthetic seismogram (respknt, ray3d)

iv) Waveform Inversion Programs using these program snglinv,smthinv, manyinv

4.7 Data Preparation

The basic idea governing receiver-function data organization is to group the signals into "clusters" that sample the same structure. Most observations are also naturally clustered by the distance and azimuth of appropriate sources.

Waves approaching a seismometer from different directions may sample very different structures. At most stations, the structure varies with azimuth and even in the simplest cases, the response can vary with distance from the station.

We usually group the observations by azimuth, then distance. We stack, or average, waveforms from the same azimuth and distance range, although at times, when the coverage is very broad, studying the response as a more continuous function of azimuth or distance is a nice way to study the structure (Ammon et al., 1997)

4.8 Data Rotation

It's often necessary and desirable to rotate traces a (figure 4-8) to form radial and transverse components of ground motion. This is possible because the SAC header has two variables that define the sense of positive ground motion for an instrument. A CMPINC = 0 indicates motion in an upward direction and a CMPINC = 90 indicates motion in a horizontal direction. The CMPAZ = 0 indicates north and CMPAZ = 90 indicates east. There is no reason that the horizontal components be oriented in such that positive motion on the horizontal component is in the north or east direction. This is often true with borehole instruments**.**

SAC is used in the rotation process when the following information is supplied.

• The event latitude and longitude

• The component azimuth

• The component incident angle

To rotate these components to the great circle and to rename the component header names KCMPNM under SAC the following commands in appendix 9

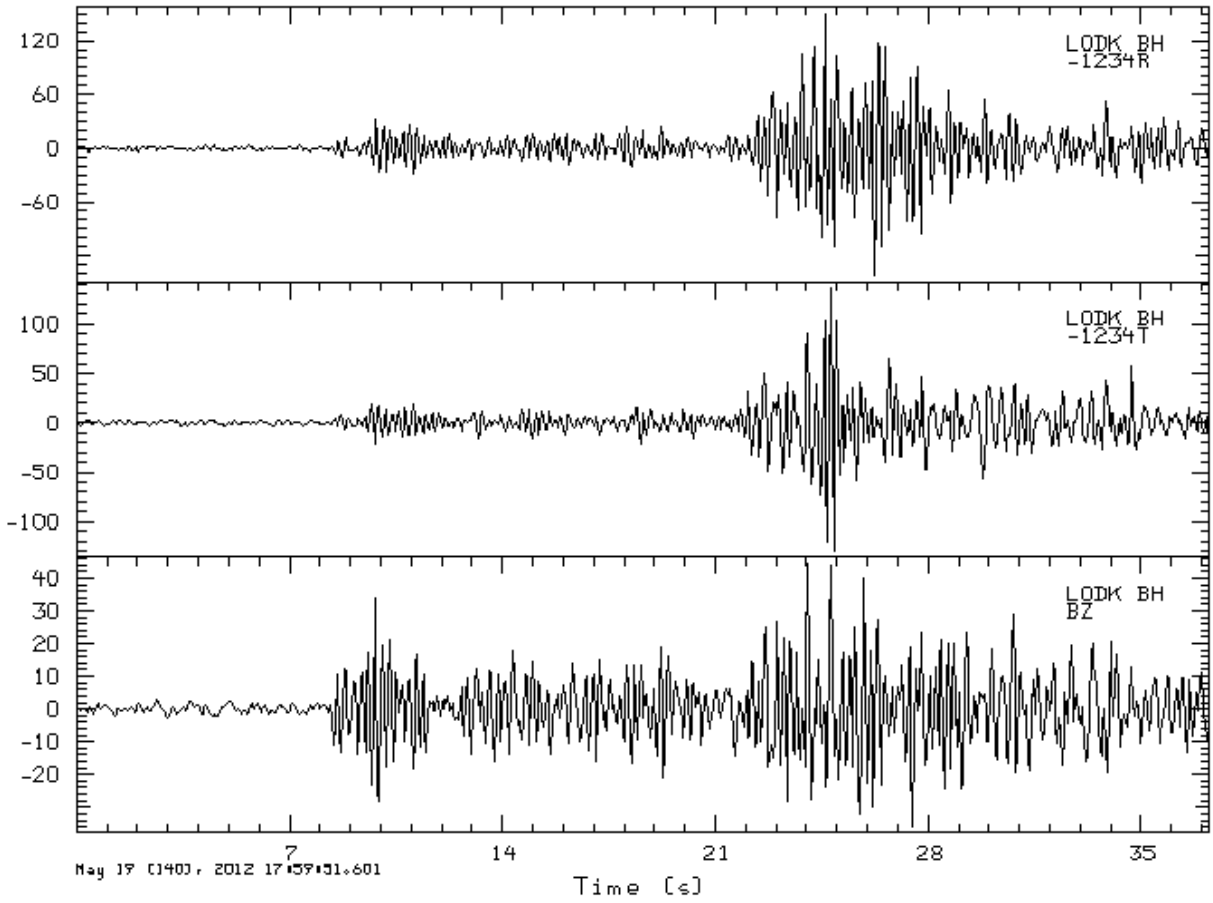

Figure 4-8: The rotate traces as LODK BHZ, LODK BHR, and LODK BHT

4.9 Windowing the Data

The final data-preparation stage consists of windowing the P waveform from the pre-signal noise and the rest of the seismic signal. The amount of record that you use depends somewhat on the seismogram. You want to isolate the P-waveform from the remaining signal. For the usual teleseismic distances (30° to 90°) you are usually safe by using about 60 seconds of signal "leader" and 60 seconds of signal following the onset of the P wave. The precise duration can vary if needed, these are typical values. At times details in the estimated receiver function may be sensitive to substantial (10s of seconds) variations in length, and you can get a feel for the variations by comparing several lengths of signal during the source equalization procedure (Ammon et al., 1997)

4.10 Isolating the Receiver Response Langston's Source Equalization Procedure

Each seismogram is a composite of source (rupture kinematics, etc.) and propagation effects (depth phases, etc). For receiver function studies, we must isolate the near-receiver structure from the source and distant structure effects. The following program iterdecon written by Charles Ammon was used as shown in appendix 7.

4.11 Creating a Velocity Model(forward model)

The starting model was created from the previous work done by KRISP 90 axial line data. The data (figure 4.9) shows that major crustal thinning occurs along the axis of the Kenya rift from moho depths of 35km in the south beneath the Kenya dome in the vicinity of Lake Naivasha to 20 km in the north beneath Lake Turkana (Mechie et al., 1993).

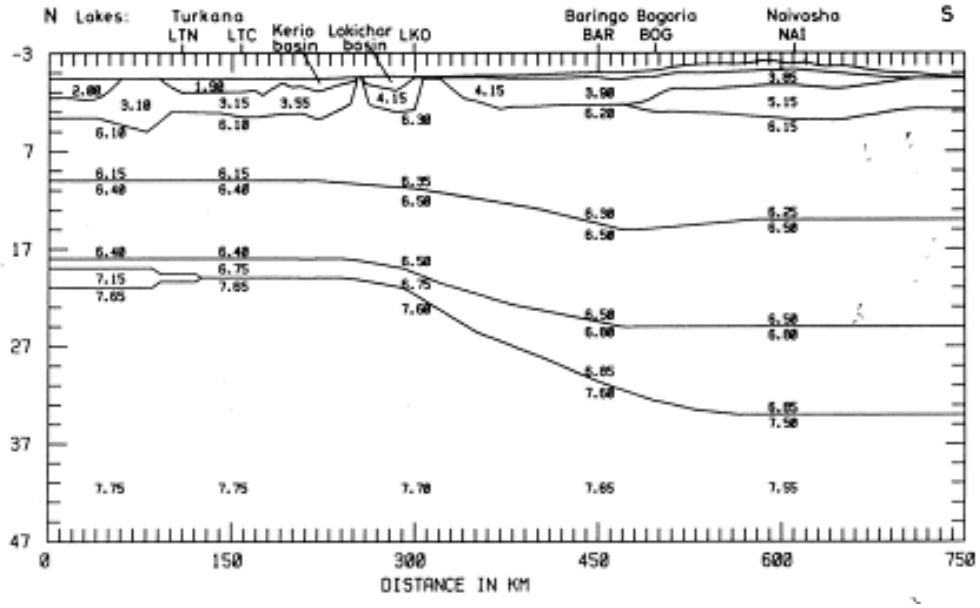

Figure 4-9: P-wave velocity model of the Earth's crust along the axis of the East African Rift in Kenya. Velocities in km/s; depths in km (from KRISP 1994)

My main area of focus was the profile along the Turkana region .The code written by Tom Owens 1991 was used to create the model. The format has spaces for Vp, Vs, density, thickness, four attenuation values, strike, dip, and Poisson's ratio. Vp and Vs are in km/s and density is in g/cm^3, the strike and dip are in decimal degrees. The

attenuation values are not used in the standard synthetic seismogram programs and so are usually left as zeros. Likewise, the value of Poisson's ratio is completely determined by Vp and Vs, and so it is not really used. Appendix 8 shows how to create model (figure 4.10) using the icmod program.

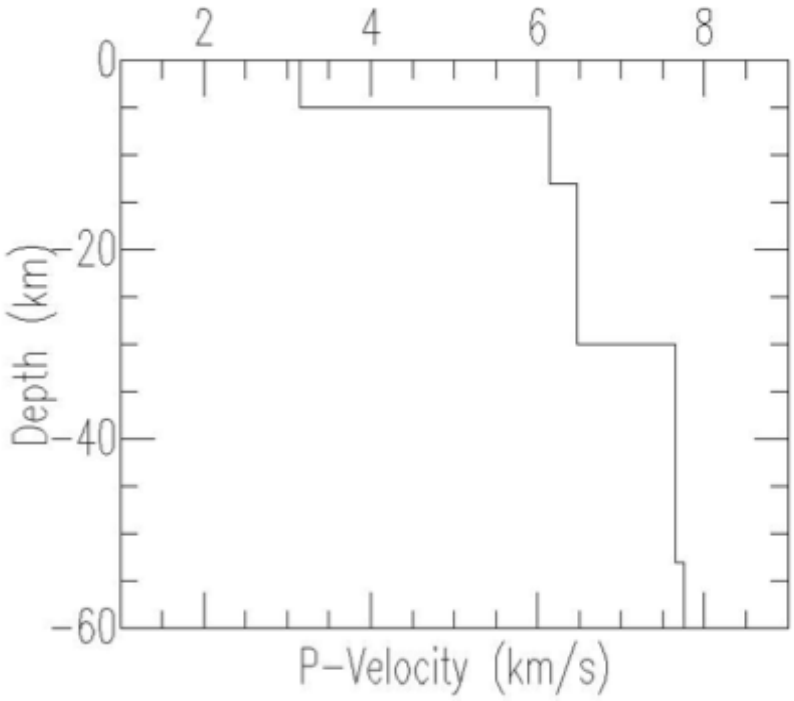

Figure 4-10: Modeled P-wave velocity model of the study area (forward model)

4.12 Waveform Inversion

There are three programs that are used to invert receiver functions: snglinv, smthinv, and manyinv. All the codes execute a linearized, iterative inversion of a specified waveform. They incorporate a minimum roughness constraint to remove non uniqueness problems from each individual inversion but the full nonlinear problem of finding acceptable models is not unique (Ammon 1997).

The procedure consists of preparing the observations, constructing an initial model, choosing a smoothness weight parameter, inverting the waveforms and assessing the significance of features in the results. The inversion is really a search for models fitting the observations using a gradient-based inversion algorithm to map out local minima. Appendix 10 gives the procedure of executing inversion.

CHAPTER FIVE

5.0 RESULTS AND DISCUSSION

5.1 Introduction

With the deployment of permanent digital three-component seismic stations in the Turkana region, teleseismic P-to-S converted waves have been studied to map the crustal thickness and the velocity of the beneath Lodwar seismic station. In this section both the processing and velocity modeling results for the receiver function analysis are presented. Only the radial component receiver function is modeled in this study. Although tangential motion can provide information on lateral structural variation (e.g., dipping interfaces), tangential receiver functions demonstrate no characteristic polarity trends with azimuthal variation. Therefore, horizontal layer parameterizations are made, and only observed radial displacement is modeled.

5.2 Results of the data from Lodwar seismic station

The receiver functions for seismic station are plotted in Figure 5-1 in a time window of between 0 to 30 s, in which the direct conversions from Moho and the crustal multiples are clearly visible. Within 4-5 second after the direct P phase, we observed the P-to-S converted phases. The most distinct phases apart from the direct phase is the multiple phase appearing 8 second after the direct P phase in figure 5.1 (a) and 7 seconds after the direct P phase in figure 5.1(b). The timing and the size of the multiple phase amplitude implies a strong velocity contrast at a depth of 15-20km below the surface (Midzi et al., 2001). A weak P_S phase is observed in the first three second after the direct P phase in figure 5.1 (a) and another weak Ps phase is observed in figure 5.1(b) at two seconds after direct P phase this is probably due to the Moho discontinuity.

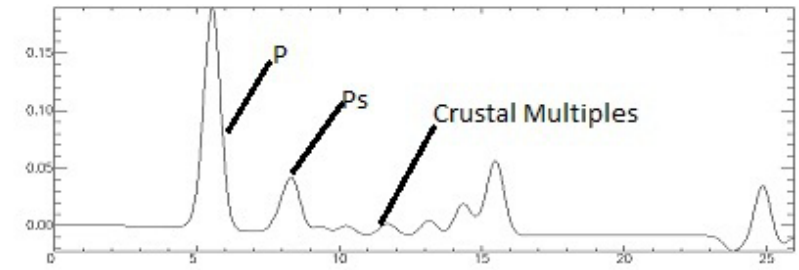

(a)

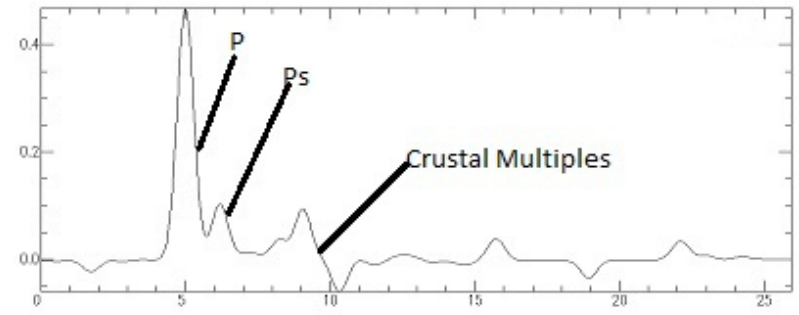

(b)

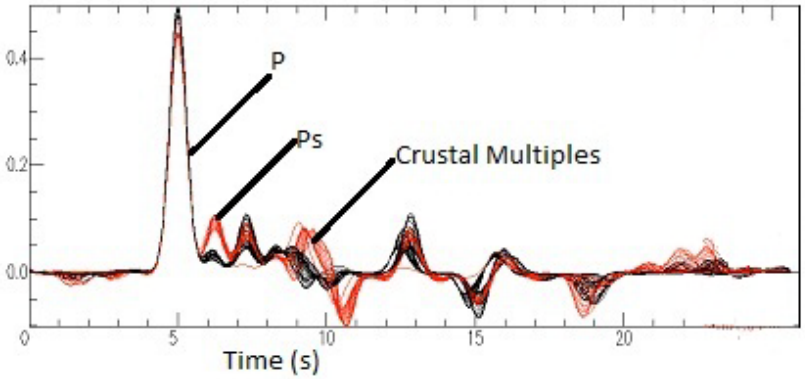

(c)

Figure 5-1: Receiver function from the station with a time window of 0 to 30 seconds

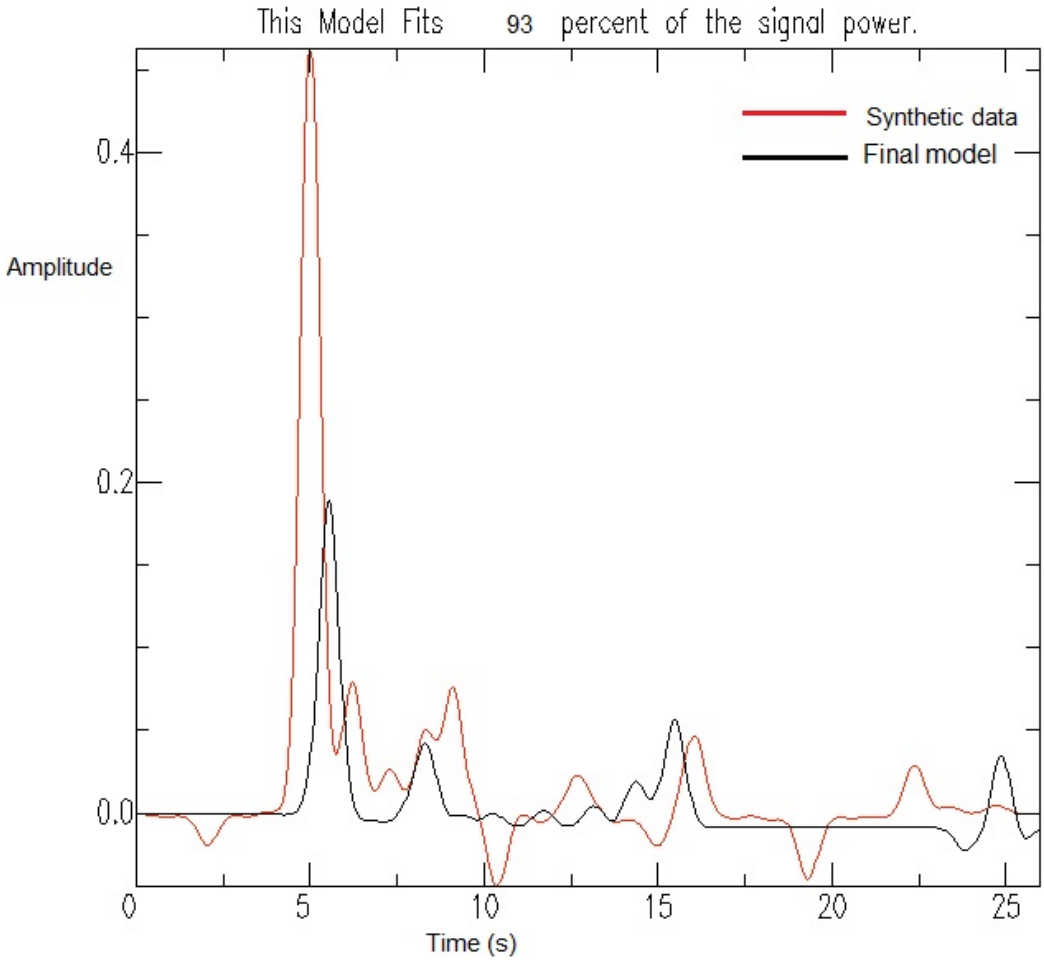

Figure 5-2: A comparison of the stacked receiver function (black line) with synthetic receiver functions (red line)

Each signal begins with an arrival of P–wave followed by P-to –S converted phases from the bottom of the surface layer. The comparison of the observed receiver function with the synthetic receiver in figure 5.2 indicates that a coherent phase at 5s and converted phase from Moho at 6s. The crustal multiples generated between the Moho and the free surface arrives at around 20s. This implies that a clear discontinuity beneath the station. The Moho depth should be similar considering the onset time of the P-to-S converted phase. The synthetic and observed receiver functions fitted well.

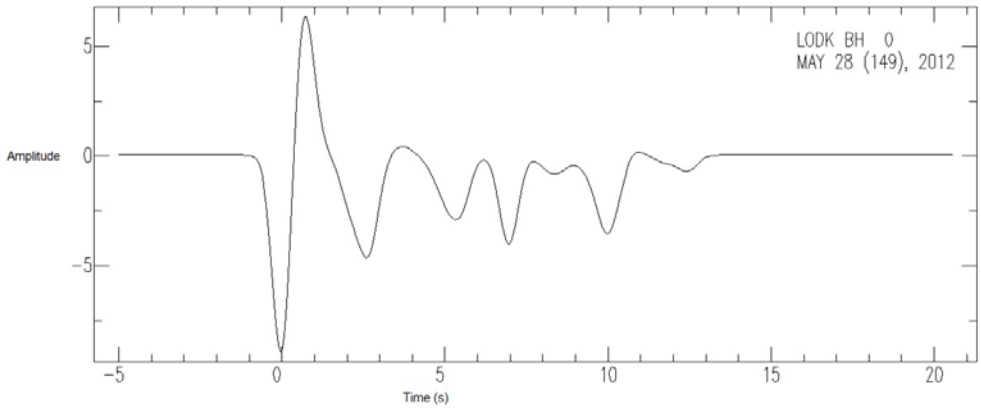

Figure 5-3: Negative Polarity

The evidence of negative (figure 5-3) peaks at 0s on the radial receiver function may be evidence of a poor receiver function. However a small set of back azimuths in this dissertation do gives a low value at 0s, this may occur if the upcoming P wave comes in perpendicular to the boundary of a dipping plate. There may also be an initial P wave offset from the 0s when you have a sediment-filled valley, as in the case of the case of Turkana basin. The model presented in this dissertation include horizontal layers, however the dipping structures such as faults are not uncommon in Turkana basin. When the waveform is coming from the direction of the dip the amplitude is high because the relative angle of this waveform to the dipping surface is more vertical.

When the waveforms are coming from a different direction from the direction of the dip then the angle between the dipping plane and the ray path is larger. Therefore, the result of deconvolution of the vertical component by the corresponding radial component has smaller amplitude. Other than the amplitudes of the second arrivals, there is another change; the presence of multiples after the Moho arrival, which exist in the synthetics generated by Model in figure 5-1(a&b).

In addition to the radial synthetic waveforms, the tangential receiver functions are often useful to determine dipping layers in the crustal structure. Tangential receiver functions indicate the dipping discontinuity by polarity changes. Based on the dip direction, the tangential receiver function from the same direction as the dip does not show any new arrivals or arrivals with smaller amplitude. However, when there are several interfaces dipping in different directions, finding the pattern in the tangential

receiver function to determine the dipping angles and directions may be very difficult. Tangential receiver function were not used in this work.

5.3 Results of Inversion

Receiver function from the station data were inverted using the domain waveform inversion scheme, this method is based on the inversion methods of Owens (1984). It is an implementation of a more efficient algorithm for calculating differential seismograms (Randall 1989) and the ‘jumping’ inversion technique of shaw and orcutt (1985) and also the method was used by Ammon et al. (1990).

Here we represent the results as p wave velocity models assuming a Poisson ratio of 0.25. An important assumption of the time domain inversion technique is that the initial model is close to the true earth velocity structure (Ammon et al., 1990). The initial model used in the inversion was derived from data from previous studies and in particular the research project by the KRISPS Kenya in the 1980’s and 1990’s.

A factor considered in the inversion is the trade-off between model roughness and rms (Ammon, 1991). Large roughness values leads to good fits. A smoothness factor of = 0.1 was observed to give realistic solutions, and also gave the same rms fit between synthetic and observed receiver function

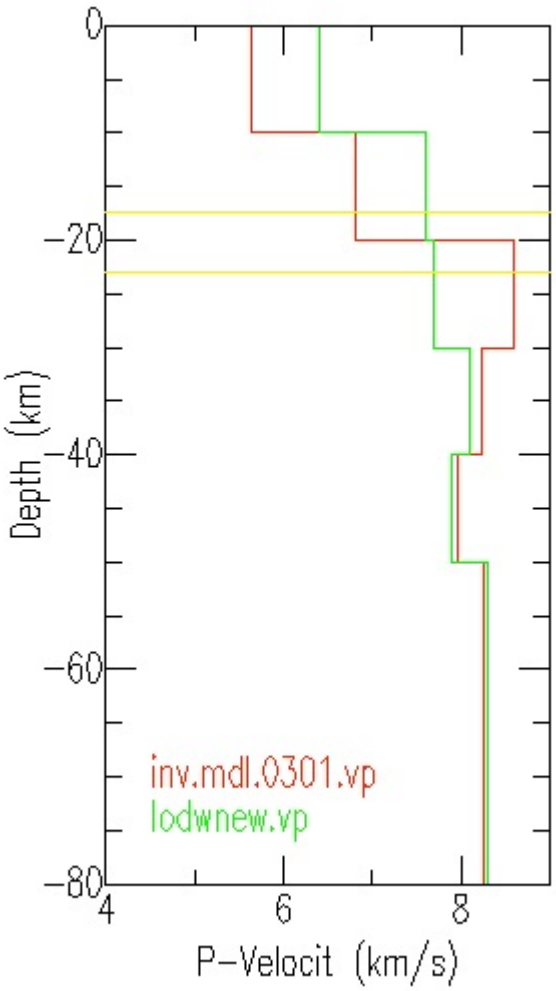

Figure 5-4: Show inversion results for Lodwar station; the black and green colors represent the initial model red solid line represents the average model after inversion.

In Figure 5.4 above, the model shows the final inversion of the receiver function. The inversion results show that the region has two main layers. The first layer is has a thickness of 10 km and an increasing P-wave velocity from 5.75 to 7.25km/s. Its lower interface coincides with the Conrad discontinuity. The second layer beneath has a thickness of 10 km with its lower interface coinciding with the Moho discontinuity. It has a P-wave increasing from 6.6 to 8.25km/s. From the previous studies (Gajewski et al., 1994) of the p_mp reflection analysis, the boundary between the upper and the lower crusts beneath the northern part of the rift occurs at about 10 km depth which agrees with the results of this investigation.

5.4 Discussion

Generally, the variation in incidence angle of the incoming seismic waves probably resulted in high dependence of receiver functions to distance and back azimuth of the events. However, Moho below the station is still observable from the station data. All synthetic receiver functions calculated from these models fitted the observed receiver functions well. The receiver function method is not sensitive to the absolute velocity of the half-space, and therefore does not provide a reliable measurement of the upper mantle velocity below the station. But in some cases the energy of the multiples (or reverberation) and the converted P-S phases is strongly dependent upon the incident angles of the seismic waves. Thus the energy of the converted Ps phases significantly increases with the incident angles. In many of the stacked data, one observed the strong Ps conversion phase 4-5s after the direct P phase. This implies a clear moho discontinuity beneath the Lodwar station.

The inversion results indicate that Moho depth is about 20 km. This figure compares quite well with the results obtained by the Kenya Rift International Seismic Project (KRISP) 1990 (Michie et al., 1993). The ability of the receiver function to resolve the P-wave velocity change at a boundary depends on the noise level in the receiver function. For records with low noise, it has been shown that the minimum velocity change (ΔVs) that can be significantly affect the P-to-S converted phase's amplitude lies between 0.2 and 0.4km/s (Cassidy 1992).

There were two major factors that were seen to influence the variation in the receiver functions beneath the seismic station. These were variation in P-to-S conversion due to Move-out and poison's ratio.

The move-out is where the P-to-S conversion arrival times caused by variation in the ray parameter of the approaching seismic waves of different events. As distance decreases from ~90^{o} to~ 30^{o}, ray parameter increases and so does the time delay between the primary P arrival and the subsequent P-to-S conversion. This came up as a result of dealing with data set of earthquake distributed over a range of distances. This was handled by accounting for the ray parameter of each event. The poison ratio (σ) of a rock body is related to the velocity of P-waves to S-waves through that body;

hence the variation in (σ) affects the time delay of P-to-S conversions in receiver functions. It was seen that a elevated (σ) causes delay in arrival times of converted phases, whilst a reduced (σ) causes converted phases to arrive early (Cassidy 1992). Advancing our understanding of crustal Poisson's ratio and Moho depths in East Africa is important because this information provides fundamental constraints on the formation and evolution of the continental crust.

Imaging crustal structure beneath the Turkana basin is not only important for determining the amount of crustal modification that may have occurred as a result of lithospheric extension, but also for improving our understanding of regional tectonism which occurred. In this region of study the thinning can be presumed to be as result of tertiary rifting episode. From the results it can also be seen that there are region with low mantle velocities. This can be readily explained in terms of partial melting of about 5 % (Achauer et al., 1994). The low p-wave velocities, less than 7.8km/s in the uppermost mantle beneath the Kenya rift, can be explained in terms of a few percent of partial melting (Keller et al., 1993).

CHAPTER SIX

6.0 CONCLUSION AND RECOMMENDATIONS

6.1 Conclusion

Receiver Functions have been proven to be a useful tool for estimating average crustal parameters in various geological settings around the world with the assumption of a 1D structure. The receiver function is a deconvolution problem, where the vertical is deconvolved with the radial in a plane layered structure. The iterative deconvolution, which has been used in this work as proved that Teleseismic receiver function analysis is now a well-established seismological technique and the most important for understanding the crustal modeling.

It extracts information to atleast the boundary between the upper and the lower mantle because it takes teleseismic wave data that have much stronger energy and longer wavelength. This method has become more sophisticated over the last two decades. Investigations are using increasing amounts of data, from ever more ambitious, wide ranging, seismological experiments; responding to the need for information regarding earthquake risk to the population. The developments in processing techniques, and data collection, allows the production of clearer and less ambiguous results regarding velocity impedance structures, and their relationship to seismogenic process.

In conclusion, we suggest that the Moho beneath the seismic station in the Turkana region is at a depth of around 20 km below the surface and a P-wave velocity increasing from 6.6 to 8.25km/s. This is basically consistent with previous studies. The study has demonstrated the usefulness of the three component broadband seismic data that is now available at university of Nairobi seismic network.

6.2 Recommendation

With the installation of more stations within the University of Nairobi Seismic Network, more studies using the receiver function need to be done to study the crustal velocity structure and infer the Moho depth at various parts of this country.

REFERENCES

Achauer, U. and Masson F. (2002). Seismic tomography of continental rifts revisited: From relative to absolute heterogeneities, *Tectonophysics*, **358**, 17–37.

Achauer, U., Glahn, A., Ritter, J.R.R., Maguire, P.K.H., Meyer, R.P., Davis, P., Slack, P. and Green, W. V. (1994). New ideas on the Kenya Rift based on the inversion of the combined dataset of the 1985 and 1989/90 seismic tomography experiments, *Tectonophysics*, **236**, 305–329.

Aki, K. & Richards, P.G., 1980. *Quantitative Seismology: Theory and Methods*, W. H. Freeman and Company, San Francisco, pp. 133–155.

Ammon, C.J., 2006. Megathrust investigations (News and Views), Nature, 440 (7080), 31-32,

Ammon C. J. and, Herrmann, R. B., 1997 Faulting Parameters of earthquake in the New Madrid, Missouri Region, Engineering Geology, 46 , 299-311,

Ammon, C.J., 1991. The isolation of receiver effects from teleseismic P waveforms, Bull. Seism. Soc. Am., 81, 2504–2510.

Ammon, C.J., Randall, G.E. and Zandt, G. (1990). On the nonuniqueness of receiver function inversions, Journal of Geophysical Research, 95, 15303–15318.

Arambourg, C., 1933 Mammiferes Miocenes du Turkana (Afrique Orientale) Ann. Paleont.22 123-146

Al-Damegh, K., Sandvol, E., and Barazangi, M., 2005. Crustal structure of the Arabian plate: New constraints from the analysis is of teleseismic receiver functions, Earth Planet. Sci. Lett., 231, 177-196.

Bath, M., and. Stefansson, R., 1966. S - P Conversions at the base of the crust, Ann. Geofis., 19, 119-130.

Benoit, M.H., Nyblade, A.A., VanDecar, J.C., 2006. Upper mantle P-wave speed variations beneath Ethiopia and the origin of the Afar hotspot. Geology 34, 329–332.

Bostock, M.G. & Cassidy, J.F., 1997. Upper mantle stratigraphy beneath the southern Slave craton, *Can. J. Earth Sci.*, **34,** 577–587.

Burke, K. & Şengör, A.M.C. 1986. Tectonic escape in the evolution of the continental crust.In: BarazangI, M(ed), Reflection Seismology, Continental Crust, Geodynamic Series, 14. American Geophysical Union Special Publication, 41–51.

Burdick, L. & Langston, C., 1977. Modeling crustal structure through the use of converted phases in teleseismic body-wave forms, bull. Seism. Soc. Am., 67 (3), 677–691.

Cassidy J.F., 1992, Numerical experiments in broadband receiver function analysis, Bull. Seism. Soc. Am, 82, p. 1453-1474.

Dawson, J.B., 1992, Neogene tectonics and volcanicity in the North Tanzania sector of the Gregory Rift Valley: Contrasts with the Kenya sector: Tecto- nophysics, v. 204, p. 81–92.

Davison, C., 1978. The founders of seismology, Arno Press, New York.

Davis, P.M. and Slack, P.D. (2002). The uppermost mantle beneath the Kenya dome and relation to melting, rifting and uplift in East Africa, *Geophysical Research Letters*, **29**(17), 1117.

Dugda, M.T., Nyblade, A.A., Julià, J., Langston, C.A., Ammon, C.J. and Simiyu, S. (2005). Crustal structure in Ethiopia and Kenya from receiver function analysis: Implications for rift development in eastern Africa. Journal of Geophysical Research, 110.

Dugda, M.T., Nyblade, A.A. and Julià, J. (2007). Thin lithosphere beneath the Ethiopian Plateau revealed by a joint inversion of Rayleigh wave group velocities and receiver functions. Journal of Geophysical Research, 12.

Dugda M.T., Nyblade A.A., Julià J. (2009) S-wave velocity structure of the crust and upper mantle beneath kenya in comparison to tanzania and ethiopia: implications for the formation of the east african and ethiopian plateaus.

Dunkleman, T. J., Karson, J. A. & Rosendahl, B. R. (1988). Structural style of the Turkana Rift. Geology 16, 258–261.

Ebinger, C. J. & Ibrahim, N. H. (1994). Multiple episodes of rifting in Central and East Africa; a re-evaluation of gravity data. Geologische
Rundschau 83, 689–702.

Freybourger, M., Gaherty, J., Jordan, T. and the Kaapvaal Seismic Group (2001). Structure of the Kaapvaal craton from surface waves. Geophysical Research Letters, 28, 2489–2492.

Foster, A., Ebinger, C., Mbede, E. and Rex, D. (1997). Tectonic development of the northern Tanzanian sector of the East African Rift system, *Journal of the Geological Society of London*, **154**, 689–700.

Fouch, M., James, D., VanDecar, J., van der Lee, S. and the Kaapvaal Seismic Group (2004). Mantle seismic structure beneath the Kaapvaal and Zimbabwe cratons. South African Journal of Geology, 10, 33–44.

Fuchs,K., Novak, O., Ritter, J.R.R., Altherr, R., Garasic, v., Volker, F., Kluge, c., Kaspar, T.(1997)An integrated model for the deep structure of the Chyulu Hills volcanic field, Kenya(from Tectonophysics, 1997, vol. 278, pages 187-209.

Furman, T., Bryce, J., Rooney, T., Yirgu, G. & Ayalew, D. (2006).Heads and tails: 30 million years of the Afar plume. In: Yirgu, G., Ebinger, C. J. & Maguire, P. K. H. (eds) The Structure and Evolution of the East African Rift System in the Afar Volcanic Province. Geological Society, London, Special Publications 259, 97–121.

Gajewski, D., Schulte, A., Riaroh, D.and Thybo, H. ., 1994. Deep seismic sounding in the Turkana Depression, northern Kenya rift. In: C Prodehl, G.R Keller and M.A

Khan (Editors), Crustal and Upper Mantle Structure of the Kenya Rift. Tectonophysics, 236: 165-178.

Green, W.V., U. Achauer, and R.P. Meyer,. 1991. A three-dimensional seismic image of the crust and upper mantle beneath the Kenya rift, *Nature, 354*, 199-203.

Gilbert, H. J., and A. F. Sheehan, 2004. Images of crustal variations in the intermountain west, Journal of Geophysical Research, v. 109.

Havskov and Ottemoller, 1999 SeisAn Earthquake analysis software, Seis. Res. Lett., 70.

Hendrie, D.B., Kusznir, N.J., Morley, C.K. and Ebinger, C.J. (1994). Cenozoic extension in northern Kenya; a quantitative model of rift basin development in the Turkana region, Tectonophysics, 236, 409–438.

James, D.E., Fouch, M.J., et al., 2001. Tectospheric structure beneath Southern Africa. Geophys. Res. Lett. 28, 2485–2488.

Juliá, J., C. J. Ammon, and A. A. Nyblade (2005), Evidence for mafic lower crust in Tanzania, East Africa, from joint inversion of receiver functions and Rayleigh wave dispersion velocities, Geophys. J. Int.

Julià, J., Ammon, C.J. and Herrmann, R.B. (2003). Lithospheric structure of the Arabian Shield from the joint inversion of receiver functions and surface-wave group velocities, *Tectonophysics*, **371**, 1–21.

Julià, J., Ammon, C.J., Herrmann, R.B. and Correig, A.M. (2000). Joint inversion of receiver functions and surface wave dispersion observations, Geophysical Journal International, 143, 99–112.

Keller, G.R., Prodehl, C., Gaciri S., Braile, L.W., Mooney, W.D.,Gajewski, D., Mechie, J.,(1992) Crustal structure beneath the Kenya Rift from axial profile data.

Keller G.R., Prodehl C., Mechie J., Fuchs K., Khan M.A., Maguire P.K.H., Mooney D.W., Achauer U., Davis.P.M., Meyer R.P., Braile L.W., Nyambok I.O., Thompson G.A., 1993 The East Africa rift system in light of KRISP 90.

Kind, R., Vinnik, L.P., 1988. The upper mantle discontinuities underneath the GRF array from P to S converted phases. J. Geophys. 62, 138–147.

Kumar, P., Yuan, X., Ravi Kumar, M., Kind, R., Li, X. and Chadha, R. (2007). The rapid drift of the Indian tectonic plate. Nature, 449, 894–897.

Langston, C.A., 1979, Structure under Mount Rainier, Washington, inferred from teleseismic body waves: Journal of Geophysical Research, v. 84, no. B9, p. 4749–4762.

Langston, C.A., 1978. Structure under Mt Rainier, Washington, Inferred from Teleseismic Body Waves. Transactions-American Geophysical Union, 59(12): 1142-1142.

Langston, C. A. (1977), Corvallis, Oregon, crustal and upper mantle structure from teleseismic P and S waves, Bull. Seismol. Soc. Am., 67, 713 – 724.

Larson, A., Snoke, J. and James, D. (2006). S-wave velocity structure, mantle xenoliths, and the upper mantle beneath the Kaapvaal Craton. Geophysical Journal International, 167, 171–186.

Last, R.J., Nyblade, A.A., Langston, C.A. and Owens, T.J. (1997). Crustal structure of the east African plateau from receiver functions and Rayleigh wave phase velocities. Journal of Geophysical Research, 102, 24469–2448.

Lay, T. and Wallace T. C., Modern global seismology, Academic Press, 1995.

Lin, F.C., M.H. Ritzwoller, Y. Yang, M.P. Moschetti, and M.J. Fouch (2011), Complex and variable crustal and uppermost mantle seismic anisotropy in the western United States, Nature Geoscience, Vol 4, Issue 1, 55-61.

Ligorria,J. P., and C. J. Ammon (1999), Iterative deconvolution and receiver-function estimation, Bull. Seismol. Soc. Am., 89, 1395–1400.

Li, A. and Burke, K. (2006). Upper mantle structure of southern Africa from Rayleigh wave tomography. Journal of Geophysical Research, 111.

MacDonald, R., Rogers, N.W., Fitton, J.G., Black, S. and Smith, M. (2001). Plume-Lithosphere Interactions in the Generation of the Basalts of the Kenya Rift, East Africa, Journal of Petrology, 42, 877–900.

McKenzie, D. P. & Bickle, M. J. (1988). The volume and composition of melt generated by extension of the lithosphere. Journal of Petrology 29, 625–679.

Mechie, J., Keller, G.R., Prodehl, C., Khan, M.A., and Gaciri, S.J., 1997, Structure and dynamic processes in the lithosphere of the Afro-Arabian Rift system: A model for the structure, composition and evolution of the Kenya Rift: Tectonophysics, v. 278, p. 95–119.

Midzi, V., Ottemoller, L., 2001. Receiver function structure beneath three southern africa seismic broadband stations. Tectonophysics 339 (3–4), 443.

Morley C.M., Ve´tel W., Le Gall B.,(2005) Inversion tectonics during continental rifting:The Turkana Cenozoic rifted zone, northern Kenya. UMR 6538 ‘‘Domaines Oce´aniques,’’ Institut Universitaire Europe´en de la Mer/CNRS-UBO, Plouzane´, France.

Morley, C. K. (1999b). Basin evolution trends in East African rifts. In C. K. Morley (Ed.), Geoscience of rift systems-evolution of East Africa (Vol. 44) (pp. 131–150). AAPG Studies in Geology.

Morley,C. K., Wescott,W.A., Stone,D.M., Harper,R. M., Wigger, S. T. & Karanja, F. M. (1992). Tectonic evolution of the northern Kenya Rift. Journal of the Geological Society, London 149, 333–348.

Nyblade, A., Knox, R. & Gurrola, H., (2000). Mantle transition zone thickness beneath Afar: implications for the origin of the Afar hotspot, Geophys. J. Crustal thinning between the Ethiopian and East African Plateaus from modeling Rayleigh wave dispersion

Nyblade, A.A. (2002). Crust and upper mantle structure in East Africa: Implications for the origin of Cenozoic rifting and volcanism and the formation of magmatic rifted

margins, *In:* M.A. Menzies, S.L. Klemperer, C.J. Ebinger and J. Baker (Editors), Volcanic Rifted Margins, *Geological Society of America*, *Special Paper*, **362**, 15–26.

Nyblade, A.A., and Langston, C.A. (2002), Broadband seismic experiments probe the East African rift, *EOS Transactions*, **83**, 405–408.

Nyblade, A.A., C. Birt, C.A. Langston, T.J. Owens, and R.J. 1996. Last, Seismic experimentreveals rifting of craton in Tanzania, *Eos Trans. AGU, 77*, 517, 520-521.

Noble, W.P., Foster, D.A., and Gleadow, A.J.W., (1997), The post–Pan-African thermal and extensional history of crystalline basement rocks in eastern Tanzania: Tec- tonophysics, v. 275, no. 4, p. 331–350.

Owens, T. J., Zandt, G., & Taylor, S. R., 1984. Seismic evidence for an ancient rift beneath the Cumberland Plateau, Tennessee: A detailed analysis of broadband teleseismic P waveforms, J. Geophys. Res., 89, 7783–7795.

Owens, T.J., Nyblade, A.A., Gurrola, H. & Langston, C.A., 2000. Mantle transition zone structure beneath Tanzania, East Africa, Geophys. Res.Lett. 27(6), 827–830.

Pasyanos, M., and Nyblade, A., (2007) A top to bottom lithospheric study of Africa and Arabia: Tectonophysics, v. 444, p. 27–44.

Pasyanos, M.E. (2005). A variable resolution surface wave dispersion study of Eurasia, North Africa, and surrounding regions, *Journal of Geophysical Research*, **110**.

Park, Y. and Nyblade, A.A. (2006). P-wave tomography reveals a westward dipping low velocity zone beneath the Kenya Rift, *Geophysical Research Letters,* **33.**

Peng, Z., Vidale, J.E., Wech, A.G., Nadeau, R.M., Creager, K.C. (2009), Remote triggering of tremor along the San Andreas Fault in central California. J. Geophys. Res. 114, 1–18.

Priestley, K., McKenzie, D., Debayle, E., and Pilidou, S., (2008), The African upper mantle and its relationship to tectonics and surface geology: Geo- physical Journal International, v. 175, p. 1108–1126.

Priestley, K., McKenzie, D. and Debayle, E. (2006). The state of the upper mantle beneath southern Africa. *Tectonophysics*, **416**, 101–112.

Priestley, K. and McKenzie, D. (2002). The structure of the upper mantle beneath Southern Africa. Geological Society Special Publications, 199, 45–64.

Prodehl, C., Ritter, J. R. R., Mechie, J., Keller, G. R., Khan, M. A., Jacob, B., Fuchs, K., Nyambok, I. O., Obel, J. D., Riaroh, D. (1997)The KRISP 94 lithospheric investigation of southern Kenya – the experiments and their main results (from Tectonophysics, vol. 278, pages 121-147.

Prodehl, C., Keller, G.R. and Khan, M.A. (1994). Crustal and upper mantle structure of the Kenya Rift: *Tectonophysics*, **236**, 1–483.

Phinney, R.A., 1964 Structure of the Earth's Crust from Spectral Behavior of Long-Period Body Waves, Jour. Geophys. Res., 69, 2997-3017.

Randall, D.E., 1989. Efficient calculation of differential seismograms for lithospheric receiver function. Geophys. J Int. 99, 469-410.

Ritter, J.R.R. and Kaspar, T. (1997). A tomography study of the Chyulu Hills, Kenya. *In:* K. Fuchs, R. Altherr, B. Müller and C. Prodehl (Editors), Structure and Dynamic Processes in the Lithosphere of the Afro-Arabian Rift System, *Tectonophysics*, **278**, 149–169.

Rondenary S., 2009. Upper mantle imaging with array recordings of converted and scattered teleseismic waves. Surv Geophys 30:377-405.

Shackleton, RM., 1986. Precambrian collission tectonic in Africa. IN:Coward ,M.P., RIES, A.C.,(Edus), collission tectonics. Geological Society of London.

Shaw, P., Orcutt, J., 1985. Waveform inversion of seismic refraction data and applications to young pacific crust. Geophys. J R. Astron.soc 82, 374-414

Slack, P.D., Davis, P.M., Dahlheim, H.A., Glahn, A., Ritter, J.R.R., Green, W.V., Maguire, P.K.H. and Meyer, R.P. (1994). Attenuation and velocity of P-waves in the mantle beneath the East African Rift, Kenya, *Tectonophysics*, **236**, 1–4, 331–358.

Stein, S. and Wysession, M., An introduction to seismology, Earthquakes and Earth Structure, Blackwell Science, 2003.

Tanya F., Kery M.K., Julia G.B., and Barry B.H., (2006) Tertiary Mafic Lavas of Turkana,Kenya:Constraints on East African Plume Structure and the Occurrence of High- m Volcanism in Africa. Journal of Petrology, Volume 47, number 6, Pages 1221–1244.

Takeuchi, H., and Saito, M. (1972). Seismic surface waves, Methods in Computational Physics, 11, 217–295.

Trabant, C. and Heinloo, A. (2004) Seiscomp 2.1 manual, GFZ Potsdam.

Van der Beek, P., Mbede, E., Andriessen, P., and Delvaux, D. (1997). Passive margin uplift around the North Atlantic region and its role in Northern Hemisphere late Cenozoic glaciation; discussion and reply, Geology, 25, 3, 282–283.

Vinnik, L. P. (1977). Detection of waves converted from P to SV in the mantle, Phys. Earth Planet. Int. 15, 39-45.

Wang, Y., Wen, L. and Weidner, D. (2008). Upper mantle SH- and P-velocity structures and compositional models beneath southern Africa. Earth and Planetary Science Letters, 267, 596–608.

Walsh, J. & Dodson, R. G. (1969). Geology of Northern Turkana. Report of the Geological Survey of Kenya 82, 42 pp.

Weeraratne, D., Forsyth, D., Fischer, K. and Nyblade, A. (2003). Evidence for an upper mantle plume beneath the Tanzanian craton from Rayleigh wave tomography. Journal of Geophysical Research, 108.

Yuan, X., R. Kind, X. Li, and R. Wang (2006), The S receiver functions: Synthetics and examples,Geophys. J. Int., 165, 555–564.

Yuan, X., Sobolev, S.V., Kind, R., Oncken, O., Bock, G., Asch, G., Schurr, B., Graeber, F., Rudloff, A., Hanka, W., Wylegalla, K., Tibi, R., Haberland, Ch., Rietbrock, A., Geiese, P., Wigger, P., Rower, P., Zandt, G., Beck, S., Wallace, T., Pardo, M., Comte. (2000). Nature (Letters). 408, 958-961

Yirgu, G., Ebinger, C.J. and Maguire, P.K.H. (Editors) (2006). The Afar Volcanic Province within the East African Rift System. Geological Society, London, Special Publications, 259pp.

Zhu, L.P., and H. Kanamori, Moho Depth Variation in Southern California from Teleseismic Receiver Functions, Jour. Geophys. Res., 105.

APPENDICES

Appendix 1: Seismic event used receiver function studies

2012-05-24-2253-38S.LODK__003_LODK__BH_E_SAC

2012-05-24-2253-38S.LODK__003_LODK__BH_N_SAC

2012-05-24-2253-38S.LODK__003_LODK__BH_R_SAC

2012-05-24-2253-38S.LODK__003_LODK__BH_T_SAC

2012-05-24-2253-38S.LODK__003_LODK__BH_Z_SAC

2012-05-28-0509-11S.LODK__003_LODK__BH_E_SAC

2012-05-28-0509-11S.LODK__003_LODK__BH_N_SAC

2012-05-28-0509-11S.LODK__003_LODK__BH_R_SAC

2012-05-28-0509-11S.LODK__003_LODK__BH_T_SAC

2012-05-28-0509-11S.LODK__003_LODK__BH_Z_SAC

2012-05-28-0517-42S.LODK__003_LODK__BH_E_SAC

2012-05-28-0517-42S.LODK__003_LODK__BH_N_SAC

2012-05-28-0517-42S.LODK__003_LODK__BH_R_SAC

2012-05-28-0517-42S.LODK__003_LODK__BH_T_SAC

2012-05-28-0517-42S.LODK__003_LODK__BH_Z_SAC

2012-06-05-1918-09S.LODK__003_LODK__BH_Z_SAC

2012-06-10-1240-11S.LODK__003_LODK__BH_E_SAC

2012-06-10-1240-11S.LODK__003_LODK__BH_N_SAC

2012-06-10-1240-11S.LODK__003_LODK__BH_R_SAC

2012-06-10-1240-11S.LODK__003_LODK__BH_T_SAC

2012-06-10-1240-11S.LODK__003_LODK__BH_Z_SAC

2012-06-11-0519-51S.LODK__003_LODK__BH_E_SAC

2012-06-11-0519-51S.LODK__003_LODK__BH_N_SAC

2012-06-11-0519-51S.LODK__003_LODK__BH_R_SAC

2012-06-11-0519-51S.LODK__003_LODK__BH_Z_SAC

2012-06-23-0442-13S.LODK__003_LODK__BH_E_SAC

2012-06-23-0442-13S.LODK__003_LODK__BH_N_SAC

2012-06-23-0442-13S.LODK__003_LODK__BH_R_SAC

2012-06-23-0442-13S.LODK__003_LODK__BH_T_SAC

2012-06-23-0442-13S.LODK__003_LODK__BH_Z_SAC

2012-06-29-2052-07S.LODK__003_LODK__BH_E_SAC

2012-06-29-2052-07S.LODK__003_LODK__BH_N_SAC

2012-06-29-2052-07S.LODK__003_LODK__BH_R_SAC

2012-06-29-2052-07S.LODK__003_LODK__BH_T_SAC

2012-06-29-2052-07S.LODK__003_LODK__BH_Z_SAC

2012-07-25-0026-03S.LODK__003_LODK__BH_E_SAC

2012-07-25-0026-03S.LODK__003_LODK__BH_N_SAC

2012-07-25-0026-03S.LODK__003_LODK__BH_R_SAC

2012-07-25-0026-03S.LODK__003_LODK__BH_T_SAC

2012-07-25-0026-03S.LODK__003_LODK__BH_Z_SAC

2012-07-26-0535-38S.LODK__003_LODK__BH_E_SAC

2012-07-26-0535-38S.LODK__003_LODK__BH_N_SAC

2012-07-26-0535-38S.LODK__003_LODK__BH_R_SAC

2012-07-26-0535-38S.LODK__003_LODK__BH_T_SAC

2012-07-26-0535-38S.LODK__003_LODK__BH_Z_SAC

2012-07-28-1957-33S.LODK__003_LODK__BH_E_SAC

2012-07-28-1957-33S.LODK__003_LODK__BH_N_SAC

2012-07-28-1957-33S.LODK__003_LODK__BH_R_SAC

2012-07-28-1957-33S.LODK__003_LODK__BH_T_SAC

2012-07-28-1957-33S.LODK__003_LODK__BH_Z_SAC

2012-08-12-1055-14S.LODK__003_LODK__BH_E_SAC

2012-08-12-1055-14S.LODK__003_LODK__BH_N_SAC

2012-08-12-1055-14S.LODK__003_LODK__BH_R_SAC

2012-08-12-1055-14S.LODK__003_LODK__BH_T_SAC

2012-08-12-1055-14S.LODK__003_LODK__BH_Z_SAC

2012-08-14-0237-15S.LODK__003_LODK__BH_E_SAC

2012-08-14-0237-15S.LODK__003_LODK__BH_N_SAC

2012-08-14-0237-15S.LODK__003_LODK__BH_R_SAC

2012-08-14-0237-15S.LODK__003_LODK__BH_T_SAC

2012-08-14-0237-15S.LODK__003_LODK__BH_Z_SAC

2012-08-18-0948-56S.LODK__003_LODK__BH_E_SAC

2012-08-18-0948-56S.LODK__003_LODK__BH_N_SAC

2012-08-18-0948-56S.LODK__003_LODK__BH_R_SAC

2012-08-18-0948-56S.LODK__003_LODK__BH_T_SAC

2012-08-18-0948-56S.LODK__003_LODK__BH_Z_SAC

2012-08-26-1508-11S.LODK__003_LODK__BH_E_SAC

2012-08-26-1508-11S.LODK__003_LODK__BH_N_SAC

2012-08-26-1508-11S.LODK__003_LODK__BH_R_SAC

2012-08-26-1508-11S.LODK__003_LODK__BH_T_SAC

2012-08-26-1508-11S.LODK__003_LODK__BH_Z_SAC

2012-08-27-0436-11S.LODK__003_LODK__BH_E_SAC

2012-08-27-0436-11S.LODK__003_LODK__BH_N_SAC

2012-08-27-0436-11S.LODK__003_LODK__BH_R_SAC

2012-08-27-0436-11S.LODK__003_LODK__BH_T_SAC

2012-08-27-0436-11S.LODK__003_LODK__BH_Z_SAC

2012-08-30-1345-06S.LODK__003_LODK__BH_E_SAC

2012-08-30-1345-06S.LODK__003_LODK__BH_N_SAC

2012-08-30-1345-06S.LODK__003_LODK__BH_R_SAC

2012-08-30-1345-06S.LODK__003_LODK__BH_T_SAC

2012-08-30-1345-06S.LODK__003_LODK__BH_Z_SAC

2012-08-31-1240-38S.LODK__003_LODK__BH_E_SAC

2012-08-31-1240-38S.LODK__003_LODK__BH_N_SAC

2012-08-31-1240-38S.LODK__003_LODK__BH_R_SAC

2012-08-31-1240-38S.LODK__003_LODK__BH_T_SAC

2012-08-31-1240-38S.LODK__003_LODK__BH_Z_SAC

2012-09-03-1822-52S.LODK__003_LODK__BH_E_SAC

2012-09-03-1822-52S.LODK__003_LODK__BH_N_SAC

2012-09-03-1822-52S.LODK__003_LODK__BH_R_SAC

2012-09-03-1822-52S.LODK__003_LODK__BH_Z_SAC

2012-09-05-1450-18S.LODK__003_LODK__BH_E_SAC

2012-09-05-1450-18S.LODK__003_LODK__BH_N_SAC

2012-09-05-1450-18S.LODK__003_LODK__BH_R_SAC

2012-09-05-1450-18S.LODK__003_LODK__BH_T_SAC

2012-09-05-1450-18S.LODK__003_LODK__BH_Z_SAC

2012-09-14-0450-15S.LODK__003_LODK__BH_E_SAC

2012-09-14-0450-15S.LODK__003_LODK__BH_N_SAC

2012-09-14-0450-15S.LODK__003_LODK__BH_R_SAC

2012-09-14-0450-15S.LODK__003_LODK__BH_T_SAC

2012-09-14-0450-15S.LODK__003_LODK__BH_Z_SAC

2012-09-30-1636-29S.LODK__003_LODK__BH_E_SAC

2012-09-30-1636-29S.LODK__003_LODK__BH_N_SAC

2012-09-30-1636-29S.LODK__003_LODK__BH_R_SAC

2012-09-30-1636-29S.LODK__003_LODK__BH_T_SAC

2012-09-30-1636-29S.LODK__003_LODK__BH_Z_SAC

2012-10-12-0034-55S.LODK__003_LODK__BH_E_SAC

2012-10-12-0034-55S.LODK__003_LODK__BH_N_SAC

2012-10-12-0034-55S.LODK__003_LODK__BH_R_SAC

2012-10-12-0034-55S.LODK__003_LODK__BH_T_SAC

2012-10-12-0034-55S.LODK__003_LODK__BH_Z_SAC

2012-10-28-0315-40S.LODK__003_LODK__BH_E_SAC

2012-10-28-0315-40S.LODK__003_LODK__BH_N_SAC

2012-10-28-0315-40S.LODK__003_LODK__BH_R_SAC

2012-10-28-0315-40S.LODK__003_LODK__BH_T_SAC

2012-10-28-0315-40S.LODK__003_LODK__BH_Z_SAC

2012-10-30-0248-25S.LODK__003_LODK__BH_E_SAC

2012-10-30-0248-25S.LODK__003_LODK__BH_N_SAC

2012-10-30-0248-25S.LODK__003_LODK__BH_R_SAC

APPENDIX 2: CREATING DATABASE IN SEISAN

First you open the terminal and locate the program SEISMO the use the command makerea as follows:

Bruces-MacBook-Pro:SEISMO bruce$ makerea

Give 1-5 letter base name, UPPER CASE

LODK

Give start time, year month, e.g. 198302

201201

Give end time, year month, e.g. 198303, blank for one month

201212

Create REA or WAV structure or BOTH

BOTH

Making directory /Users/bruce/SEISMO/REA/LODK_

Making directory /Users/bruce/SEISMO/REA/LODK_/LOG

Making directory /Users/bruce/SEISMO/REA/LODK_/CAT

Making directory /Users/bruce/SEISMO/REA/LODK_/2012

Making directory /Users/bruce/SEISMO/REA/LODK_/2012/01

Making directory /Users/bruce/SEISMO/REA/LODK_/2012/02

Making directory /Users/bruce/SEISMO/REA/LODK_/2012/03

Making directory /Users/bruce/SEISMO/REA/LODK_/2012/04

Making directory /Users/bruce/SEISMO/REA/LODK_/2012/05

Making directory /Users/bruce/SEISMO/REA/LODK_/2012/06

Making directory /Users/bruce/SEISMO/REA/LODK_/2012/07

Making directory /Users/bruce/SEISMO/REA/LODK_/2012/08

Making directory /Users/bruce/SEISMO/REA/LODK_/2012/09

Making directory /Users/bruce/SEISMO/REA/LODK_/2012/10

Making directory /Users/bruce/SEISMO/REA/LODK_/2012/11

Making directory /Users/bruce/SEISMO/REA/LODK_/2012/12

After you with make the database, then return to copy the events files in the /WOR directory.

Bruces-MacBook-Pro:LODW bruce$ cd ..

Bruces-MacBook-Pro:WOR bruce$ cd LODW

Bruces-MacBook-Pro:LODW bruce$ dirf 2*

1 2012-05-19-0536-01S.LODK__003

2 2012-05-19-1807-36S.LODK__003

3 2012-05-20-0148-24S.LODK__002

4 2012-05-20-0729-39S.LODK__002

5 2012-05-22-0012-44S.LODK__003

6 2012-05-22-0307-53S.LODK__003

7 2012-05-22-0307-57S.LODK__003

Appendix 3: Autoreg (registering data in Seisan)

Bruces-MacBook-Pro:LODW bruce$ AUTOREG

Bruces-MacBook-Pro:LODW bruce$ AUTOREG

Event type for all events: Local: L (default)

Regional: R

Distant: D

L

Move (m) or copy (c) waveform files to WAV (enter=n)?

M

1-5 letter base name, return for standard base,,, for local base

LODK

Operator, max 4 chars

bkm

The last part of the command output looks something like this:

2012-05-19-0536-01S.LODK__003

sfile: /Users/bruce/SEISMO/REA/LODK_/2012/05/19-0536-01L.S201205

/Users/bruce/SEISMO/REA/LODK_/2012/05/19-0536-01L.S201205

2012-05-19-1807-36S.LODK__003

sfile: /Users/bruce/SEISMO/REA/LODK_/2012/05/19-1807-36L.S201205

/Users/bruce/SEISMO/REA/LODK_/2012/05/19-1807-36L.S201205

sfile: /Users/bruce/SEISMO/REA/LODK_/2012/05/20-0729-39L.S201205

/Users/bruce/SEISMO/REA/LODK_/2012/05/20-0729-39L.S201205

Now your \REA directory has the LODK database, with folders for each month.

Appendix 4: Parameter file for Seisan

```
RESET TEST(02)=500.0
RESET TEST(07)=-1.2
RESET TEST(08)=1.9
RESET TEST(09)=0.0004
RESET TEST(11)=99.0
RESET TEST(13)=5.0
RESET TEST(34)=1.5
RESET TEST(35)=2.5
RESET TEST(36)=0.0
RESET TEST(41)=20000.0
RESET TEST(43)=5.0
RESET TEST(51)=3.6
RESET TEST(50)=1.0
RESET TEST(56)= 1.0
TEST(58)= 99990.0
RESET TEST(40)=0.0
RESET TEST(60)=0.0
RESET TEST(71)=1.0
RESET TEST(75)=1.0
RESET TEST(76)=0.910
RESET TEST(77)=0.00087
RESET TEST(78)=-1.67
RESET TEST(79)=1.0
RESET TEST(80)=3.0
RESET TEST(81)=1.0
RESET TEST(82)=1.0
RESET TEST(83)=1.0
RESET TEST(88)=1.0
RESET TEST(85)=0.1
RESET TEST(91)=0.1
KMBO 1.1268S 37.2523E    1940
FURI   8.8952N 38.6798E    2570
NAI    1.2739S 36.8037E     1713
KIBK   2.3591S 38.0433E      790
LODK  3.4219N 35.3616E       665
MAG    155.08S 3617.40E      660
```

APPENDIX 5: Working in SEISAN using EEV in the working directory

The following is an example from the data used here, in which we select one month (201205) of the event database for our events:

Bruces-MacBook-Pro: ~ bruce$ cd SEISMO/

Bruces-MacBook-Pro:SEISMO bruce$ wo

Bruces-MacBook-Pro:WOR bruce$ eev 201205 LODK_

2012 5 Reading events from base LODK_ 13

1 19 May 2012 0: 0 18 L ? P

Read headers from files:

/Users/bruce/SEISMO/WAV/LODK_/2012/05/2012-05-19-0000-18S.BKM1__003

Plot options: Interactive picking Return

Multi trace plot on screen, def (0)

Multi trace plot on screen (1)

Multi trace plot on screen+laser (2)

Multi trace plot on laser (3)

Continuoues on screen (4)

Continuoues on screen + laser (5)

Continuoues on laser (6)

Stop (q)

APPENDIX 6: CONVERSION OF DATA FROM SEISAN TO SAC

```
Bruces-MacBook-Pro: 05 bruce$ dirf 2*
 # 1 2012-05-19-0000-18S.BKM1__003
 # 2 2012-05-20-0000-22S.BKM1__002
 # 3 2012-05-21-0000-23S.BKM1__002
 # 4 2012-05-22-0000-00S.BKM1__003
 # 5 2012-05-23-0000-00S.BKM1__003
Bruces-MacBook-Pro:05 bruce$ sacsei
  (1) Sac (ASCII or BINARY) -> seisan binary
  (2) seisan binary -> sac binary
  Choice ?
2
 Filename or number, filenr.lis for all
1
  number of traces:           3
 trace:           1
LODK BH E 2012 5 19 0 0 18.05
 Channel # and name not defined in def file:   1 LODK BH E
  SAC output filename: 2012-05-19-0000-18S.BKM1__003_LODK__BH_E_SAC
 trace:           2
LODK BH N 2012 5 19 0 0 29.70
 Channel # and name not defined in def file:   1 LODK BH N
  SAC output filename: 2012-05-19-0000-18S.BKM1__003_LODK__BH_N_SAC
 trace:           3
LODK BH Z 2012 5 19 0 0 30.70
 Channel # and name not defined in def file:   1 LODK BH Z
  SAC output filename: 2012-05-19-0000-18S.BKM1__003_LODK__BH_Z_SAC
 Filename or number, filenr.lis for all
```

Appendix 7: Iterdecon (for performing deconvolution)

```
SAC> iterdecon
 Program iterdeconfd - Version 1.04, 1997-98
 Chuck Ammon, Saint Louis University
 What is the numerator file?
2012-05-28-0517-42S.LODK__003_LODK__BH_R_SAC
 What is the denominator file?
2012-05-28-0517-42S.LODK__003_LODK__BH_Z_SAC
 What is the max number of iterations?
200
 What is the phase shift (secs) for the output?
5.0
 What is minimum percent error increase to accept?
0.001
 What is is the Gaussian filter width factor?
2.5
 Allow negative pulses? (1->y, 0->no)
1
 Minimal (0) or verbose output (1)?
0
The maximum spike delay is    6.40000
 File        Spike amplitude   Spike delay   Misfit   Improvement
 r001         -.170604789E+01       .300     3.48%     96.5186%
 r002          .167911872E+00      5.950     2.55%      .9350%
 r003          .771043301E-01       .000    2.35%      .1971%
 r004          .313025340E-01      6.300     2.32%      .0325%
 r005         -.273744017E-01      3.700     2.29%      .0249%
 r006          .229299907E-01      4.900     2.27%      .0174%
 r007          .270717330E-01      1.550     2.25%      .0243%
 r008         -.167764928E-01      3.650     2.24%      .0093%
 r009          .175310224E-01      4.850     2.23%      .0102%
Last Error Change =     .0009%
 Hit the min improvement tolerance - halting.
 Number of bumps in final result:  37
 The final deconvolution reproduces   97.8% of the signal.
```

The receiver function not recovering at least 85% of the original waveform were rejected.

APPENDIX 8: Icmod (for creating starting model)

```
SAC> icmod
 your options are:
   1 -- input all parameters for each layer
   2 -- same as 1 except default qp,qs,strk,dip
   3 -- input pv & poissons ratio; same defaults as 2
   4 -- input sv & poissons ratio; same defaults as 2
   5 -- same as 3 except default rho and poissons rat
   6 -- same as 4 except default rho and poissons rat
 please input option no.
5
 choose between:
   1 -- inputting layer thkness, or
   2 -- depth to bottom of layer.
1
 choose between:
   1 -- tjo output format
   2 -- srt output format, or
   3 -- output in both formats.
1
 input is in free format, type 0.0 for h/z to end input
 lyr
 vp  h/z
   1
3.15,5
   2
6.15,8
   3
6.48,17
   4
7.65,23
   5
7.75,0.0
 lyr    vp      vs      rho     h/z     qp      qs      strk   dip     por
  1   3.1500  1.8187  1.7780  5.0000  0.0000  0.0000  0.0000  0.0000  0.2500
  2   6.1500  3.5507  2.7380  8.0000  0.0000  0.0000  0.0000  0.0000  0.2500
  3   6.4800  3.7412  2.8436 17.0000  0.0000  0.0000  0.0000  0.0000  0.2500
  4   7.6500  4.4167  3.2180 23.0000  0.0000  0.0000  0.0000  0.0000  0.2500
  5   7.7500  4.4745  3.2500  0.0000  0.0000  0.0000  0.0000  0.0000  0.2500
are these ok?  y
output file name?   vellod
title?    velocity lodwar
SAC> vplot
velocity file  vellod
List the site model? (y or n) y
 file: vellod     model:  velocity     5 layers
 lyr     vp      vs     rho      h     qp      qs     strike    dip
   1     3.15    1.82    1.78    5.00    0.00    0.00    0.00    0.00
   2     6.15    3.55    2.74    8.00    0.00    0.00    0.00    0.00
   3     6.48    3.74    2.84   17.00    0.00    0.00    0.00    0.00
```

```
  4     7.65    4.42    3.22   23.00    0.00    0.00    0.00    0.00
  5     7.75    4.47    3.25    0.00    0.00    0.00    0.00    0.00
SAC> r vellod.vp
SAC> xvp .1 .5
SAC> xlim 1 9
SAC> ylim -60 0
SAC> xlabel "P-Velocity @(km/s@)"
SAC> ylabel "Depth @(km@)"
SAC> axes on t l
SAC> gt si m
SAC> fileid off
SAC> p
```

APPENDIX 9: Data Rotation

SAC> r 2012-05-24-2253-38S.LODK_*

2012-05-24-2253-38S.LODK__003_LODK__BH_E_SAC 2012-05-24-2253-38S.LODK__003_LODK__BH_N_SAC 2012-05-24-2253-38S.LODK__003_LODK__BH_Z_SAC

SAC> chnhdr evlo 178.015

SAC> chnhdr evla 83.841

SAC> chnhdr stlo 35.3616

SAC> chnhdr stla 3.4219

SAC> writehdr append

SAC> r 2012-05-24-2253-38S.LODK__003_LODK__BH_N_SAC

SAC> ch CMPAZ 0 CMPINC 90

SAC> wh

SAC> r 2012-05-24-2253-38S.LODK__003_LODK__BH_E_SAC

SAC> ch CMPAZ 90 CMPINC 90

SAC> wh

SAC> r 2012-05-24-2253-38S.LODK__003_LODK__BH_N_SAC 2012-05-24-2253-38S.LODK__003_LODK__BH_E_SAC

SAC> rotate to GCP

SAC> w 2012-05-24-2253-38S.LODK__003_LODK__BH_R_SAC 012-05-24-2253-38S.LODK__003_LODK__BH_T_SAC

SAC> r 2012-05-24-2253-38S.LODK__003_LODK__BH_Z_SAC 2012-05-24-2253-38S.LODK__003_LODK__BH_R_SAC 012-05-24-2253-38S.LODK__003_LODK__BH_T_SAC

SAC> qdp off

SAC> p1

SAC> q

Appendix 10: Working with inversion program Manyinv

```
seismologylab4@seismologylab4-Lenovo-Product:~/Desktop/LODSAC/rotated/GoodOnes/2012-08-26-1508$ ls
2012-08-26-1508-11S.LODK__003_LODK__BH_R_SAC  decon.out      observed
vellod.rho
2012-08-26-1508-11S.LODK__003_LODK__BH_T_SAC  denominator    predicted
vellod.vp
2012-08-26-1508-11S.LODK__003_LODK__BH_Z_SAC  numerator      vellod
vellod.vs
seismologylab4@seismologylab4-Lenovo-Product:~/Desktop/LODSAC/rotated/GoodOnes/2012-08-26-1508$ snglinv
 snglinv - Receiver function inversion program.
          VERSION 2.1 July 1997
     Charles J. Ammon and George Randall.
 Additional routines by George Zandt and Tom Owens.
 Inversion run on: Fri Oct 18 14:05:46 2013
 Maximum Number of points in each waveform = 512
  input velocity model:
Newvel
Enter the max number of iterations per inversion
5
 Enter the smoothing trade-off parameter
0.1
 Enter inversion ID number (for output naming)
1
 Enter Singular Value truncation fraction
0.001
Apply a high-pass filter to waveforms? n
 Enter number of seismograms:
1
 Enter sac file name:
decon.out
 Enter the horizontal slowness:
0.06
 Enter the delay:
5.0
 Enter the gaussian width factor:
2.5
 Read in:
  i  name             p     tdelay    gauss
 01  decon.out         0.060    5.000  2.50
 Inversion Input Parameters:
 Initial Velocity Model: vellod
 Max Number of Iterations:           5
 Smoothing trade-off parameter:   0.100000001
 Singular-Value Truncation Fraction:    1.00000005E-03
 Inversion ID Number:  01
 Inversion Diagnostics:
 Initial Model Vp over Vs Ratio
 Layer   Vp/Vs       Poissons Ratio
```

```
  1   1.7320064       0.250
  2   1.7320529       0.250
  3   1.7320646       0.250
  4   1.7320625       0.250
  5   1.7320371       0.250
Iteration:          0
Initial fractional square misfit:    3.86891079
Initial rms errors:   0.103122868
Initial roughness alpha, beta:   1.73006761      0.998832643
Iteration:          1
SVD truncation summary:
Truncation fraction:    1.00000005E-03
Max Singular Value:    12.7762785
Min Singular Value:    1.00937986
Min Singular Value used    1.00937986
Condition Number (smax / smin):    12.6575527
# parameters, # SV used, # truncated
         5          5          0
Fractional square misfit:    2.61425209
rms errors:    8.47684741E-02
Roughness alpha, beta:   1.60924888      0.929102898
Percent Roughness Change (alpha,beta):    93.02    107.51
 Iteration:          2
SVD truncation summary:
Truncation fraction:    1.00000005E-03
Max Singular Value:    11.4356670
Min Singular Value:    1.00956893
Min Singular Value used    1.00956893
Condition Number (smax / smin):    11.3272772
# parameters, # SV used, # truncated
         5          5          0
Fractional square misfit:    2.37923479
rms errors:    8.08684826E-02
Roughness alpha, beta:   1.39114749      0.803182065
Percent Roughness Change (alpha,beta):    80.41    124.36
Iteration:          3
SVD truncation summary:
Truncation fraction:    1.00000005E-03
Max Singular Value:    10.9945650
Min Singular Value:    1.00960481
Min Singular Value used    1.00960481
Condition Number (smax / smin):    10.8899689
# Parameters, # SV used, # truncated
         5          5          0
Fractional square misfit:    2.34638143
rms errors:    8.03082064E-02
Roughness alpha, beta:   1.64782619      0.951375544
Percent Roughness Change (alpha,beta):    95.25    104.99

Iteration:          4
```

SVD truncation summary:
Truncation fraction: 1.00000005E-03
Max Singular Value: 11.5123215
Min Singular Value: 1.00968826
Min Singular Value used 1.00968826
Condition Number (smax / smin): 11.4018574
Parameters, # SV used, # truncated
5 5 0
Fractional square misfit: 2.33092237
rms errors: 8.00432190E-02
Roughness alpha, beta: 1.55017900 0.894998312
Percent Roughness Change (alpha,beta): 89.60 111.60
Iteration: 5
SVD truncation summary:
Truncation fraction: 1.00000005E-03
Max Singular Value: 10.9023237
Min Singular Value: 1.00960839
Min Singular Value used 1.00960839
Condition Number (smax / smin): 10.7985668
Parameters, # SV used, # truncated
5 5 0
Fractional square misfit: 2.30954742
rms errors: 7.96753690E-02
Roughness alpha, beta: 1.64294267 0.948555648
Percent Roughness Change (alpha,beta): 94.96 105.30
Final Model

Layer	Vp/Vs	Poissons Ratio
1	1.7320064	0.250
2	1.7320529	0.250
3	1.7320646	0.250
4	1.7320626	0.250
5	1.7320371	0.250

APPENDIX 11: SAC HEADER

```
% sac                          # launch sac again
SAC> r lodk.EHZ.SAC            # read the data again
SAC> lh                        # list the SAC header
  FILE: lodk.EHZ.SAC - 1
 ----------
    NPTS = 2409                # number of data points
       B = -9.992996e+00       # begin time
       E = 1.408700e+01        # end time
  IFTYPE = TIME SERIES FILE    # file type
   LEVEN = TRUE                # evenly sampled time series
   DELTA = 1.000000e-02        # time increment
    IDEP = VELOCITY (NM/SEC)   # physical unit of the data
  DEPMIN = -2.073471e+04       # minimum amplitude
  DEPMAX = 1.584818e+04        # maximum amplitude
  DEPMEN = 5.137106e+01        # mean amplitude
 OMARKER = 0                   # event origin marker
 AMARKER = 1.848               # first arrival (P) marker
T0MARKER = 3.192               # t0 (S) marker
  KZDATE = NOV 20 (324), 1999  # reference date
  KZTIME = 00:12:55.840        # reference time
  IZTYPE = GMT DAY             # type of reference time
   KSTNM = BV                  # station name
   CMPAZ = 0.000000e+00        # component azimuth relative to north
  CMPINC = 0.000000e+00        # component "incidence angle" reletive
                                 to the vertical
    STLA = 4.075520e+01        # station latitude
    STLO = 3.101490e+01        # station longitude
    STEL = 2.470000e+0         # station elevation
    STDP = 0.000000e+0         # station depth below surface (meters)
    EVLA = 4.079930e01         # event latitude
    EVLO = 3.100330+01         # event longitude
    EVDP = 8.15000e+00         # event depth
    DIST = 4.99444e+00         # source receiver distance in km
      AZ = 1.68686e+02         # azimuth
     BAZ = 3.48961e+02         # back azimuth
   GCARC = 4.42941e-02         # great circle distance
  LOVROK = TRUE                # TRUE if it is okay to overwrite this
                                 file on disk
   USER7 = 0.000000e+00        # User defined time picks
   USER8 = 0.000000e+00        # User defined time picks
   NVHDR = 6                   # Header version number. Current value
                                 is the integer 6.
   SCALE = 1.000000e+00        # Multiplying scale factor for
                                 dependent variable [not currently
                                 used]
   NORID = 0                   # Origin ID (CSS 3.0)
   NEVID = 0                   # Event ID (CSS 3.0)
   NWFID = 2                   # Waveform ID (CSS 3.0)
  LPSPOL = FALSE               # TRUE if station components have a
                                 Positive polarity (left-hand rule)
  LCALDA = TRUE                # TRUE if DIST, AZ, BAZ, and GCARC are
                                 to be calculated from station and
                                 event coordinates
  KCMPNM = EPZ_01              # Component name
     MAG = 2.310000e+00        # Event magnitude
```

Appendix 12: Data used in the Analysis

Date(yymmdd)	Time(hrminsec)	Latidute	Longitude	Magnitude
20120524	225338	83.492	178.015	5
20120528	50911	-82.841	31.872	5.1
20120528	51742	-1.154	-22.834	5
20120611	51951	-9.68	74.178	5.3
20120623	44213	48.871	104.159	5
20120725	2603	-34.234	115.335	5.9
20120726	53538	-0.874	-21.67	5.7
20120728	195733	79.279	54.544	5
20120814	23715	43.368	-79.135	6.6
20120818	94856	48.683	-10.021	5
20120826	150811	43.726	-59.057	5.8
20120827	43611	18.553	41.991	5
20120830	134506	20.783	-47.285	5.5
20120831	124038	49.689	130.152	7
20120905	145018	8.966	-6.51	5.8
20120914	45015	0.43	119.735	5.6
20120930	163629	35.391	3.581	5.5
20121012	3455	73.73	114.279	5.7